Paper:
Aria, A., Rabczuk, T. & Friswell, M. (2019). A finite element model for the thermo-elastic analysis of functionally graded porous nanobeams. *European Journal of Mechanics - A/Solids*
http://dx.doi.org/10.1016/j.euromechsol.2019.04.002

A finite element model for the thermo-elastic analysis of functionally graded porous nanobeams

Arash Imani Aria, Timon Rabczuk, Michael Ian Friswell

PII: S0997-7538(19)30008-7

DOI: https://doi.org/10.1016/j.euromechsol.2019.04.002

Reference: EJMSOL 3767

To appear in: *European Journal of Mechanics / A Solids*

Received Date: 3 January 2019

Revised Date: 27 February 2019

Accepted Date: 1 April 2019

Please cite this article as: Aria, A.I., Rabczuk, T., Friswell, M.I., A finite element model for the thermo-elastic analysis of functionally graded porous nanobeams, *European Journal of Mechanics / A Solids* (2019), doi: https://doi.org/10.1016/j.euromechsol.2019.04.002.

A Finite Element Model for the Thermo-Elastic Analysis of Functionally Graded Porous Nanobeams

Arash Imani Aria[a,1], Timon Rabczuk[b,c], Michael Ian Friswell[d,]

[a]Tabriz University, Department of Mechanical Engineering, Tabriz, Iran.
[b]Department of Civil Engineering, Bauhaus University Weimar, Weimar, Germany.
[c]Institute of Research and Development, Duy Tan University, Da Nang 550000, Vietnam.
[d]Swansea University, Bay Campus, Fabian Way, Swansea SA1 8EN, UK.

Abstract

In this study, for the first time, a nonlocal finite element model is proposed to analyse thermo-elastic behaviour of imperfect functionally graded porous nanobeams (P-FG) on the basis of nonlocal elasticity theory and employing a double-parameter elastic foundation. Temperature-dependent material properties are considered for the P-FG nanobeam, which are assumed to change continuously through the thickness based on the power-law form. The size effects are incorporated in the framework of the nonlocal elasticity theory of Eringen. The equations of motion are achieved based on first-order shear deformation beam theory through Hamilton's principle. Based on the obtained numerical results, it is observed that the proposed beam element can provide accurate buckling and frequency results for the P-FG nanobeams as compared with some benchmark results in the literature. The detailed variational and finite element procedure are presented and numerical examinations are performed. A parametric study is performed to investigate the influence of several parameters such as porosity volume fraction, porosity distribution, thermal loading, material graduation, nonlocal parameter, slenderness ratio and elastic foundation stiffness on the critical buckling temperature and the nondimensional fundamental frequencies of the P-FG nanobeams. Based on the results of this study, a porous FG nanobeam has a higher thermal buckling resistance and natural frequency compared to a perfect FG nanobeam. Also, uniform distributions of porosity result in greater critical buckling temperatures and vibration frequencies, in comparison with functional distributions of porosities.

Keywords: Thermal buckling; Thermal vibration; Porous functionally graded nanobeam; Finite elements; Nonlocal elasticity.

1. Introduction

Developing nano and micro-technologies have enabled the design of many nano/micro-structures with a wide range of functions and applications. In this category, there are many nano/micro-systems that work in thermal environments and under thermal stresses, which may lose their functionality due to problems such as phase changing. In order to overcome these difficulties functionally graded materials (FGMs) would be a great solution, which are able to stay stable in ultra-high temperatures [1,2].

[1] Corresponding author E-mail address: arashimaniaria@gmail.com.

The enhanced mechanical, chemical, and electronic properties of nano/micro-structural elements, such as nano/micro-scale beams and plates, motivates the analysis of these small scale structures where the size effects are significant. Hence, the study of nanostructures has gained immense interest by scientists in recent years. There are two major methods to model nanostructures, namely molecular dynamic (MD) simulations and continuum mechanics. However, MD simulations require great computational effort to model the nanostructures with many atoms and classical continuum mechanics theory is unable to incorporate size effects in micro/nano scale structures, which results in over prediction of their responses [3-9]. In order to overcome these problems, Eringen's nonlocal elasticity theory [10], which is the most popular high-order continuum mechanics theory, may be the best solution. This non-classical theory captures size effects with high accuracy [10-15] in modelling micro and nano structures. The basis of Eringen's nonlocal elasticity theory is that the stress state at a given point is not only a function of the strain at that specific point, but also is a function of the strain at all other adjacent points of the continuum. Consequently, this theory is able to simulate the long range forces between atoms and molecules [10].

A novel class of composite materials are functionally graded materials (FGMs), which have been used in many engineering applications. Employing FGMs can remove interface difficulties and relieve thermal stress concentrations in structural components, that are the main problems with typical laminated composites. The advantageous properties of FGMs are naturally achieved as their material composition changes gradually and continuously as a function of position in specific spatial directions [16,17,18]. Generally, an FGM is build-up of two distinct material constituents, such as ceramic and metal phases. In an FGM, the ceramic component is chosen as a high temperature resistor, due to its low thermal conductivity, where the metal constituent is a ductile material, which can avoid fracture caused by thermal stresses. Recently, some outstanding studies on the examination of vibration and buckling of FG nano structures by employing high-order continuum theories (nonlocal elasticity) have been reported. Using the third order plate theory, Daneshmehr and Rajabpoor [19] analysed the static stability of nonlocal FG plates, considering different boundary conditions. The resonance frequencies of FG micro/nanoplates were investigated by Nami and Janghorban [20] on the basis of the nonlocal elasticity and strain gradient theory. Based on their research, each of these two size dependent approaches can be interpreted with distinct physical meaning of the small scale structures. The free vibrations of FG Timoshenko nanobeams in the framework of nonlocal elasticity using Navier's solution was analysed by Rahmani and Pedram [21]. Later, the thermoelastic behaviour of an FG Timoshenko nanobeam was studied by Ebrahimi and Salari [22], using nonlocal elasticity theory and Navier's solution. They investigated the free transverse vibrations of nanobeams employing Euler-Bernoulli theory (EBT) and a semi-analytical differential transform method, considering gradually varying material distribution [23]. In a separate work, they analysed thermo-mechanical vibration of compositionally graded EBT nanobeams with various boundary conditions exploiting a semi-analytical differential transform method [24]. Nejad et al. [25] used the generalised differential quadrature method (GDQM) and proposed a solution for the static stability problem of EBT nanobeams made of two-directional FGMs. A similar solution was also employed by Ansari et al. [26] to analyse the thermal vibration response of postbuckled piezoelectric Timoshenko nanobeams based on nonlocal elasticity theory. Ebrahimi et al. [27]

examined the thermomechanical vibrations of FG nano beams based on stress gradient theory by investigating various boundary conditions. Nguyen et al. [28] used a computational approach to investigate the bending, buckling and vibration of FG nanoplates based on a quasi-3D theory. Shafiei et al. [29] examined the vibration of bi-dimensional perfect and imperfect FG porous nano/micro-beams, utilizing GDQM in the framework of nonlocal elasticity and modified coupled stress theory.

In addition to these analytical and computational studies, there are a few investigations which have used FEM to study the vibration and static responses of FGMs. Proposing a new beam element, Chakraborty et al. [30] investigated the vibration behaviour of FGMs, considering thermal effects, based on first-order shear deformation theory. Eltaher et al. [31] developed a two-noded and six degrees-of-freedom FE element to examine the free vibration of FG nanobeams in the framework of nonlocal elasticity theory, employing Euler-Bernoulli beam theory. Later, in a distinct work, the same two-noded element was employed by Eltaher et al. [32] to analyse the static response and stability of FG nanobeams. Aria and Friswell [33] proposed a novel 5-noded nonlocal beam element to investigate vibration and buckling behaviour of FG nanobeams.

Porous materials are also a unique kind of material with an increasing number of applications. Recently, many scientists have shown interest in studying the mechanical properties of these types of materials [34-37]. Also, the dynamic behaviour of porous materials has attracted the attention of some researchers. Bo [38] examined the transverse vibration of elastic circular plates embedded in fluid-saturated porous half spaces. The damped vibration response of automotive double walls with porous materials was investigated by Yamaguchi et al. [39] employing the finite element method (FEM). The bending vibrations of a thin rectangular porous plate saturated by a fluid was examined by Leclaire et al. [40], using classical plate theory (CPT). Using energy methods, Vashishth and Gupta [41] analysed the transverse vibration of an anisotropic porous piezoelectric ceramic plate. The dynamic responses of heterogeneous porous micro materials were investigated by Altintas [42]. Takahashi and Tanaka [43] studied a theoretical method for the acoustic coupling caused by bending vibrations of porous elastic plates. The electro-thermo-mechanical vibrational response of porous FG piezoelectric plates was investigated by Barati and Zenkour [44] using a refined four-variable plate theory. The nonlinear static bending of FG porous micro/nano-beams with uniform porosities was studied by Sahmani et al. [45]. Also, in another investigation [46], they analysed the vibration response of FG porous micro/nano-beams reinforced with graphene platelets. Khoei et al. [47] employed an enriched FEM to simulate hydraulic fracturing procedure in fractured porous media. Mobasher et al. [48] proposed a new non-local model for transport and damage in porous media. Na and Sun [49], presented a finite strain model for frozen porous media on the basis of multiplicative kinematics.

Thermal buckling and vibration often occur in many structures, and these phenomena should be considered to ensure structural safety. Thus, thermoelastic investigations of beam structures are common in structural mechanics' analysis. Most of the literature in the area of FGMs ignore the influences of the thermal environment, elastic medium and porosity in their analysis. To the best of the authors' knowledge, this paper for the first time, proposes a nonlocal Timoshenko finite element model to study the thermoelastic buckling and vibrational behaviour of imperfect FG porous nanobeams embedded in a double-parameter elastic foundation on the basis of nonlocal elasticity theory. The material distribution is applied as a through-thickness power-law variation. Hamilton's principal is employed to derive the weak form of the equations, including the boundary conditions. Critical buckling loads and natural frequencies are obtained for various boundary conditions, nonlocal parameters, porosity distributions, material graduations and span to depth ratios by using a 5-noded beam element.

2. Formulation

2.1. Porosity-dependent functionally graded materials in thermal environments

For a P-FGM beam (Fig. 1), the material properties change continuously along the z direction, and are considered as [29]

$$P(z) = (P_m - P_c)\left(\frac{z}{h}+\frac{1}{2}\right)^k + P_c - \frac{\lambda}{2}(P_m + P_c) \tag{1}$$

Here, k denotes the non-negative power-law exponent, λ is the porosity volume fraction and P_c and P_m show the corresponding material properties of the ceramic and metal constituents. The Young's modulus, $E(z)$, shear modulus, $G(z)$, material density $\rho(z)$ and thermal expansion coefficient $\alpha(z)$, of FGM-I (uniformly distributed porosity) are defined based on this material graduation function as

$$E(z) = (E_m - E_c)\left(\frac{z}{h}+\frac{1}{2}\right)^k + E_c - \frac{\lambda}{2}(E_m + E_c) \tag{2}$$

$$G(z) = (G_m - G_c)\left(\frac{z}{h}+\frac{1}{2}\right)^k + G_c - \frac{\lambda}{2}(G_m + G_c) \tag{3}$$

$$\rho(z) = (\rho_m - \rho_c)\left(\frac{z}{h}+\frac{1}{2}\right)^k + \rho_c - \frac{\lambda}{2}(\rho_m + \rho_c) \tag{4}$$

$$\alpha(z) = (\alpha_m - \alpha_c)\left(\frac{z}{h}+\frac{1}{2}\right)^k + \alpha_c - \frac{\lambda}{2}(\alpha_m + \alpha_c) \tag{5}$$

Considering the functional porosity distribution (FGM-II), the relations of Young's modulus, $E(z)$, shear modulus, $G(z)$, material density $\rho(z)$ and thermal expansion coefficient $\alpha(z)$, in Eqs. (2)-(5) will be defined in new forms as [29]

$$E(z) = (E_m - E_c)\left(\frac{z}{h}+\frac{1}{2}\right)^k + E_c - \frac{\lambda}{2}(E_m + E_c)(1 - \frac{2|z|}{h}) \tag{6}$$

$$G(z) = (G_m - G_c)\left(\frac{z}{h}+\frac{1}{2}\right)^k + G_c - \frac{\lambda}{2}(G_m + G_c)(1 - \frac{2|z|}{h}) \tag{7}$$

$$\rho(z) = (\rho_m - \rho_c)\left(\frac{z}{h}+\frac{1}{2}\right)^k + \rho_c - \frac{\lambda}{2}(\rho_m + \rho_c)(1 - \frac{2|z|}{h}) \tag{8}$$

$$\alpha(z) = (\alpha_m - \alpha_c)\left(\frac{z}{h}+\frac{1}{2}\right)^k + \alpha_c - \frac{\lambda}{2}(\alpha_m + \alpha_c)(1 - \frac{2|z|}{h}) \tag{9}$$

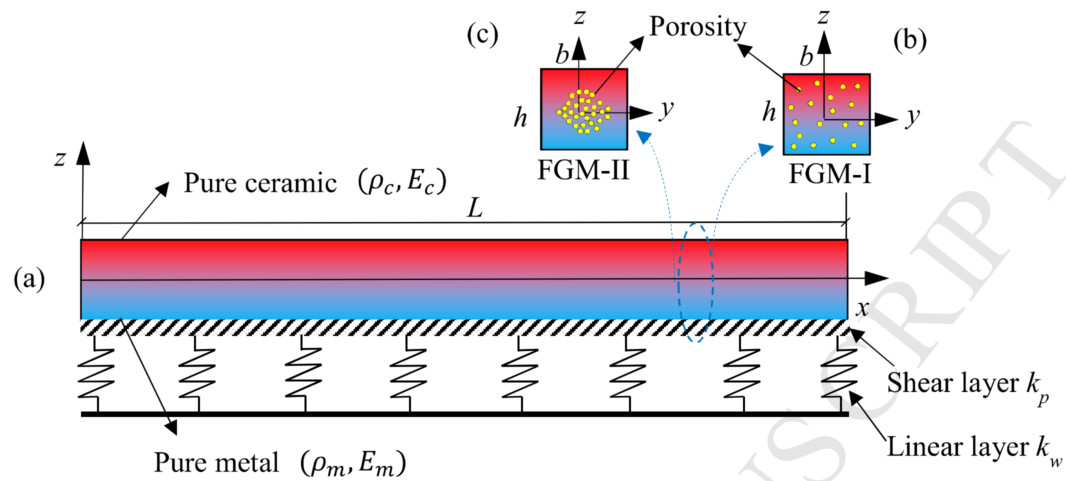

Fig. 1 (a) Geometry of a porous functionally graded beam on a Winkler-Pasternak medium, (b) uniform distribution of porosities (FGM-I), (c) functional distribution of porosities (FGM-II).

Based on the P-FG beam defined in Eq. (1), the upper and lower faces of the nanobeams are ceramic-rich and metal-rich, respectively, and their material properties are given in Table 1. The geometry of a P-FG nanobeam on a Winkler-Pasternak foundation is shown in Fig. 1.

The use of FGMs in high temperature environments results in unavoidable changes in material properties. Accurate calculations of the response of FGMs at high temperatures, requires the consideration of the temperature dependency of the material properties. The nonlinear equation of thermo-elastic material properties as a function of temperature T(K) can be defined as [50]

$$P = P_0(P_{-1}T^{-1} + 1 + P_1T^1 + P_2T^2 + P_3T^3) \tag{10}$$

where P_0, P_{-1}, P_1, P_2 and P_3 are coefficients for the temperature, T(K), that are given in Table 1 for different material properties of Si_3N_4 and $SUS304$.

Table 1. Temperature dependent coefficients of Young's modulus E (Pa), thermal expansion coefficient α (1/K), Poisson's ratio ν, and mass density ρ (kg/m3) for various materials [51].

Materials	P_0	P_{-1}	P_1	P_2	P_3	P at 300 K
Si_3N_4						
E	348.43e+9	0	-3.070e-4	2.160e-7	-8.946e-11	322.27e+9
α	5.8723e-6	0	9.095e-4	0	0	7.475e-6
υ	0.24	0	0	0	0	0.24
ρ	2370	0	0	0	0	2370
$SUS304$						
E	201.04e+9	0	3.079e-4	-6.534e-7	0	207.79e+9
α	12.330e-6	0	8.086e-4	0	0	15.321e-6
υ	0.3262	0	-2.002e-4	3.797e-7	0	0.318
ρ	8166	0	0	0	0	8166

2.2 Nonlocal elasticity theory

In nonlocal elasticity theory [5], the stress at a point $\mathbf{x}$ in an elastic body depends not only on the strain at that specific point, but also on the strain at all points in the body. Thus, the nonlocal stress tensor is given by

$$\boldsymbol{\sigma} = \int_V \alpha_0(\boldsymbol{x}, \boldsymbol{x}', e_0 a)\boldsymbol{C}(\boldsymbol{x}') : \boldsymbol{\varepsilon}(\boldsymbol{x}')dV \quad (11)$$

Here, α_0 is the principal attenuation kernel function, which defines the constitutive equations for the nonlocal influences at the reference point $\boldsymbol{x}$ produced by the local strain at the source $\boldsymbol{x}'$. $e_0 a$ shows the nonlocal parameter, which incorporates the nonlocal elastic stress field, where e_0 is a constant appropriate to each material and a is an internal characteristic length. $\boldsymbol{C}$ is the fourth-order elasticity tensor, $\boldsymbol{\varepsilon}$ is the strain tensor, V is the volume of the continuum and ":" designates the double-dot product of tensors.

Although, to date, no agreement has been achieved on how to specify the material-dependent length scale parameter experimentally, some studies have extracted the nonlocal parameter by molecular dynamics simulations in CNTs [52,53,54]. In this paper a parametric study is performed to analyse the effect of this parameter on the vibration behaviour of FG porous nanobeams.

The solution of Eq. (11) is complicated. However, the linear nonlocal differential operator may be used for the exponential nonlocal kernel function, i.e., $\mathbb{L} = 1 - (e_0 a)^2 \nabla^2$. Employing this operator in Eq. (11), the following relation is derived

$$(1 - (e_0 a)^2 \nabla^2)\boldsymbol{\sigma} = \boldsymbol{C} : \boldsymbol{\varepsilon} \tag{12}$$

where, $\nabla^2 = \frac{\partial^2}{\partial x^2}$ is the Laplacian operator.

For a beam like structure, the nonlocal behavior in the thickness direction can be neglected. Therefore, the nonlocal constitutive relations take the form:

$$\sigma_{xx} - (e_0 a)^2 \frac{\partial^2 \sigma_{xx}}{\partial x^2} = E(z)\varepsilon_{xx} \tag{13}$$

$$\sigma_{xz} - (e_0 a)^2 \frac{\partial^2 \sigma_{xz}}{\partial x^2} = G(z)\gamma_{xz} \tag{14}$$

where σ_{xx} is the axial normal stress, σ_{xz} is the shear stress, ε_{xx} is the axial strain and γ_{xz} is the shear strain, $E(z)$ is the elasticity modulus and $G(z)$ is the shear modulus of the P-FG beams. The constitutive relations for the classical (local) theory are obtained by setting $e_0 a = 0$.

2.3 Timoshenko beam theory based on nonlocal elasticity

The displacement field of a Timoshenko beam is defined as

$$u_x(x,z,t) = u(x,t) - z\phi(x,t) \tag{15}$$

$$u_y(x,z,t) = 0, \tag{16}$$

$$u_z(x,z,t) = w(x,t) \tag{17}$$

Here, u and w denote the displacement components of the mid-surface in the x and z directions, respectively, and ϕ is the slope and t denotes the time. The Timoshenko strains are given by

$$\varepsilon_{xx} = \frac{\partial u_x}{\partial x} = \frac{\partial u}{\partial x} - z\frac{\partial \phi}{\partial x} \tag{18}$$

$$\gamma_{xz} = \frac{1}{2}\left(\frac{\partial w}{\partial x} - \phi\right) \tag{19}$$

$$\varepsilon_{yy} = \varepsilon_{zz} = \gamma_{xy} = \gamma_{yz} = 0. \tag{20}$$

In order to derive equation of motion, Hamilton’s principle is exploited

$$\delta \int_{t_1}^{t_2} [T - (U + W_e + V^T)]dt = 0 \tag{21}$$

where U, W_e, V^T and T are the strain energy, the potential energy of the external forces, the potential energy caused by the thermal stress and the kinetic energy, respectively. The variation of the strain energy is

$$\delta U = \int_V \sigma_{ij}\, \delta\epsilon_{ij} dV = \int_V (\sigma_{xx}\, \delta\epsilon_{xx} + \sigma_{xz}\delta\gamma_{xz})dV \tag{22}$$

The stress resultants are expressed as

$$N_{xx} = b\int_A \sigma_{xx}\,(z)dz, \quad M_{xx} = b\int_A z\sigma_{xx}(z)\,dz, \quad Q_{xz} = b\int_A \sigma_{xz}(z)\,dz \tag{23}$$

where A is the cross section area. The variation of the strain energy in terms of the stress resultants, is

$$\delta U = \int_0^L \left(N_{xx}\frac{\partial \delta u}{\partial x} - M_{xx}\frac{\partial \delta\phi}{\partial x} + Q_{xz}\frac{\partial \delta w}{\partial x} - Q_{xz}\delta\phi\right)dx \tag{24}$$

The variation of the kinetic energy is given as

$$\delta T = \int_0^L \rho(z)A\frac{\partial u_x}{\partial t}\delta\left(\frac{\partial u_x}{\partial t}\right)dx + \int_0^L \rho(z)A\frac{\partial u_z}{\partial t}\delta\left(\frac{\partial u_z}{\partial t}\right)dx$$

$$=\int_0^L (m_0\frac{\partial u}{\partial t} - m_1\frac{\partial \phi}{\partial t})\delta\left(\frac{\partial u}{\partial t}\right)dx + \int_0^L (m_2\frac{\partial \phi}{\partial t} - m_1\frac{\partial u}{\partial t})\delta\left(\frac{\partial \phi}{\partial t}\right)dx + \int_0^L (m_0\frac{\partial w}{\partial t})\delta\left(\frac{\partial w}{\partial t}\right)dx \tag{25}$$

where the mass moments of inertia are given by

$$\begin{Bmatrix} m_0 \\ m_1 \\ m_2 \end{Bmatrix} = b\int_{-h/2}^{h/2} \begin{Bmatrix} 1 \\ z \\ z^2 \end{Bmatrix} \rho(z)dz \tag{26}$$

The variation of the work done by the external forces is expressed as

$$\delta W_e = -\iiint_V (f\delta u + q\delta w)dV \tag{27}$$

Here, f and q are the axial distributed forces and the transverse distributed forces, respectively.

Assuming the P-FG beam has been in a thermal environment for a long period of time, then the temperature distribution can be considered to be uniform across the beam thickness. Hence, in this study, a uniform temperature gradient is analysed. Also, the temperature is assumed to rise from the stress free state temperature T_0 to the final temperature ΔT. Thus, the thermal stresses occur in the P-FG as

$$\sigma_{xx}^T = \sigma^T = -E(z)\alpha(z)\Delta T \tag{28}$$

$$\sigma_{xy}^T = 0. \tag{29}$$

where σ_{xx}^T is the thermal axial stress and σ_{xy}^T is the thermal shear stress. The variation of the potential energy caused by the thermal stress can be written as [55]

$$\delta V^T = -\int_0^L A_{xx}^T \left(\frac{\partial u}{\partial x}\frac{\partial \delta u}{\partial x} + \frac{\partial w}{\partial x}\frac{\partial \delta w}{\partial x}\right) dx \tag{30}$$

where the thermal stress can be written as

$$A_{xx}^T = \int_{-h/2}^{h/2} \sigma^T dz \tag{31}$$

By substituting Eqs. (24), (25), (27) and (30) into Eq. (21), performing integration by parts, and setting the coefficients of δu, $\delta\phi$ and δw equal to zero, the equations of motion for a Timoshenko beam are deduced as

$$\delta u : \frac{\partial N_{xx}}{\partial x} - m_0 \frac{\partial^2 u}{\partial t^2} + m_1 \frac{\partial^2 \phi}{\partial t^2} - A_{xx}^T \frac{\partial^2 u}{\partial x^2} + f = 0 \tag{32}$$

$$\delta\phi : Q_{xz} - \frac{\partial M_{xx}}{\partial x} - m_2 \frac{\partial^2 \phi}{\partial t^2} + m_1 \frac{\partial^2 u}{\partial t^2} = 0 \tag{33}$$

$$\delta w : \frac{\partial Q_{xz}}{\partial x} - m_0 \frac{\partial^2 w}{\partial t^2} + q - A_{xx}^T \frac{\partial^2 w}{\partial x^2} = 0 \tag{34}$$

The corresponding boundary conditions, resulting from the above mathematical process at $x = 0$ and $x = L$, are deduced as

$$\delta u \Longrightarrow \text{either} \quad N_{xx} - A_{xx}^T \frac{\partial u}{\partial x} = 0 \quad \text{or} \quad u = 0 \tag{35}$$

$$\delta\phi \Rightarrow \text{either} \quad M_{xx} = 0 \quad \text{or} \quad \phi = 0 \tag{36}$$

$$\delta w \Rightarrow \text{either} \quad Q_{xz} - A_{xx}^T \frac{\partial w}{\partial x} = 0 \quad \text{or} \quad w = 0 \tag{37}$$

Substituting Eqs. (18) and (15) into Eqs. (13) and (14), and employing Eq. (23), the corresponding stress resultants can be obtained as

$$N_{xx} = (ea_0)^2 \frac{\partial^2 N_{xx}}{\partial x^2} + (A_{xx} \frac{\partial u}{\partial x} - B_{xx} \frac{\partial \phi}{\partial x}), \tag{38}$$

$$Q_{xz} = (ea_0)^2 \frac{\partial^2 Q_{xz}}{\partial x^2} + k_s A_{xz} (\frac{\partial w}{\partial x} - \phi), \tag{39}$$

$$M_{xx} = (ea_0)^2 \frac{\partial^2 M_{xx}}{\partial x^2} + \left(B_{xx} \frac{\partial u}{\partial x} - D_{xx} \frac{\partial \phi}{\partial x}\right). \tag{40}$$

where, the extensional coefficient A_{xx}, the extensional–bending coefficient B_{xx}, the bending coefficient D_{xx} and the shear coefficient A_{xz} are given by

$$\begin{Bmatrix} A_{xx} \\ B_{xx} \\ D_{xx} \end{Bmatrix} = b \int_{-h/2}^{h/2} \begin{Bmatrix} 1 \\ z \\ z^2 \end{Bmatrix} E(z) dz \tag{41}$$

$$A_{xz} = b \int_{-h/2}^{h/2} G(z) dz \tag{42}$$

In view of Eqs. (32)-(34), Eqs. (38)-(40) can be expressed in displacement form as

$$N_{xx} = (ea_0)^2 (m_0 \frac{\partial^3 u}{\partial x \partial t^2} - m_1 \frac{\partial^3 \phi}{\partial x \partial t^2} - \frac{\partial f}{\partial x} - A_{xx}^T \frac{\partial^2 u}{\partial x^2}) + (A_{xx} \frac{\partial u}{\partial x} - B_{xx} \frac{\partial \phi}{\partial x}), \tag{43}$$

$$Q_{xz} = (ea_0)^2 (m_0 \frac{\partial^3 w}{\partial x \partial t^2} - \frac{\partial q}{\partial x} - A_{xx}^T \frac{\partial w}{\partial x} \frac{\partial^3 w}{\partial x^3}) + k_s A_{xz} (\frac{\partial w}{\partial x} - \phi), \tag{44}$$

$$M_{xx} = (ea_0)^2 (m_0 \frac{\partial^2 w}{\partial t^2} - m_2 \frac{\partial^3 \phi}{\partial x \partial t^2} + m_1 \frac{\partial^3 u}{\partial x \partial t^2} + \frac{\partial f}{\partial x} - A_{xx}^T \frac{\partial^2 w}{\partial x^2} - q) + \left(B_{xx} \frac{\partial u}{\partial x} - D_{xx} \frac{\partial \phi}{\partial x}\right). \tag{45}$$

Here, $k_s = 5/6$ designates the shear correction factor.

Substituting Eqs. (43)-(45) into Eqs. (32)-(34) the governing equations of motion with respect to the displacements for a Timoshenko beam is achieved as

$$\left(A_{xx} \frac{\partial^2 u}{\partial x^2} - B_{xx} \frac{\partial^2 \phi}{\partial x^2}\right) = (1 - (ea_0)^2 \frac{\partial^2}{\partial x^2})(m_0 \frac{\partial^2 u}{\partial t^2} - m_1 \frac{\partial^2 \phi}{\partial t^2} - f - A_{xx}^T \frac{\partial^2 u}{\partial x^2}), \tag{46}$$

$$\left(k_s A_{xz} \frac{\partial w}{\partial x} - k_s A_{xz} \phi - B_{xx} \frac{\partial^2 u}{\partial x^2} + D_{xx} \frac{\partial^2 \phi}{\partial x^2}\right)$$

$$= (ea_0)^2 \left(m_1 \frac{\partial^4 u}{\partial x^2 \partial t^2} - m_2 \frac{\partial^4 \phi}{\partial x^2 \partial t^2}\right) + m_2 \frac{\partial^2 \phi}{\partial t^2} - m_1 \frac{\partial^2 u}{\partial t^2}. \tag{47}$$

$$k_s A_{xz} \left(\frac{\partial^2 w}{\partial x^2} - \frac{\partial \phi}{\partial x}\right) = (1 - (ea_0)^2 \frac{\partial^2}{\partial x^2})(m_0 \frac{\partial^2 w}{\partial t^2} - q - A_{xx}^T \frac{\partial^2 w}{\partial x^2}), \tag{48}$$

By multiplying Eqs. (46)-(48) by δu , $\delta\phi$ and δw respectively, and performing integration over the beam length, the weak form is deduced as

$$\int_0^L \Big[\Big(A_{xx}\frac{\partial u}{\partial x}\frac{\partial \delta u}{\partial x} - B_{xx}\frac{\partial \phi}{\partial x}\frac{\partial \delta u}{\partial x}\Big) - \Big(1-(ea_0)^2\frac{\partial^2}{\partial x^2}\Big)\Big(m_0\frac{\partial^2 u}{\partial t^2}\delta u - m_1\frac{\partial^2 \phi}{\partial t^2}\delta u + f\delta u - A_{xx}^T\frac{\partial u}{\partial x}\frac{\partial \delta u}{\partial x}\Big) + \big(-k_s A_{xz}\frac{\partial w}{\partial x}\delta\phi + k_s A_{xz}\phi\delta\phi - B_{xx}\frac{\partial u}{\partial x}\frac{\partial \delta\phi}{\partial x} + D_{xx}\frac{\partial \phi}{\partial x}\frac{\partial \delta\phi}{\partial x}\big) + \Big(1-(ea_0)^2\frac{\partial^2}{\partial x^2}\Big)\big(-m_1\frac{\partial^2 u}{\partial t^2}\delta\phi + m_2\frac{\partial^2 \phi}{\partial t^2}\delta\phi\big) + k_s A_{xz}\big(-\phi\frac{\partial \delta w}{\partial x} + \frac{\partial w}{\partial x}\frac{\partial \delta w}{\partial x}\big) + \Big(1-(ea_0)^2\frac{\partial^2}{\partial x^2}\Big)\big(m_0\frac{\partial^2 w}{\partial t^2}\delta w + q\delta w - A_{xx}^T\frac{\partial w}{\partial x}\frac{\partial \delta w}{\partial x}\big)\Big]dx = 0. \tag{49}$$

In Eq. (49), by neglecting the time dependent terms, the weak form related to buckling can be obtained.

2.4 Finite element formulation

A five-node beam element, with four equally spaced nodes and one node at the middle is shown in Fig. 2. This element has ten degrees-of freedom including three axial, three rotational and four transverse displacements, which are defined at the neutral axis. Hence, the nodal displacement vector is given by

$$\boldsymbol{q} = \{u_1\ u_2\ u_3\ \ w_1\ w_2\ w_3\ w_4\ \phi_1\ \phi_2\ \phi_3\}^T \tag{50}$$

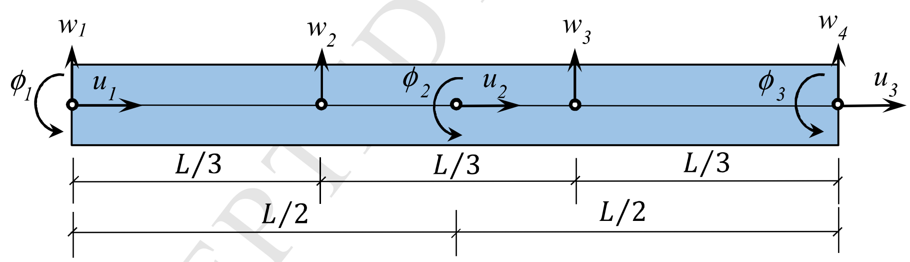

Fig. 2 Beam element with ten degrees of freedom.

The domain of the beam is discretized into a number of elements. The weak form is considered for each of the discrete elements of length L with domain $\mho^e = (x_e, x_{e+1})$. By assuming the solutions
$u(x,t) = \sum_{i=1}^{3} u_i\varphi_i(x)e^{i\omega t}$, $w(x,t) = \sum_{i=1}^{4} w_i\psi_i(x)e^{i\omega t}$, $\phi(x,t) = \sum_{i=1}^{3} \phi_i\theta_i(x)e^{i\omega t}$ with no axial forces and $q = k_p\frac{\partial^2 w}{\partial x^2} - k_w w$, where k_w is the linear stiffness of the Winkler medium, k_p is the shear stiffness related to the Pasternak medium, A is the cross section area, α is the linear thermal expansion coefficient and ΔT is the temperature change, one achieves the general form of Eq. (49) for all nodes of a single element, as

$$\int_0^L \Big[\Big(A_{xx}\frac{\partial\varphi}{\partial x}\frac{\partial\delta\varphi}{\partial x} - B_{xx}\frac{\partial\theta}{\partial x}\frac{\partial\delta\varphi}{\partial x}\Big) + \Big(1-(ea_0)^2\frac{\partial^2}{\partial x^2}\Big)\Big(m_0\omega^2\varphi\delta\varphi - m_1\omega^2\theta\delta\varphi - A_{xx}^T\frac{\partial\varphi}{\partial x}\frac{\partial\delta\varphi}{\partial x}\Big) + (k_sA_{xz}\theta\delta\theta - k_sA_{xz}\frac{\partial\psi}{\partial x}\delta\theta - B_{xx}\frac{\partial\varphi}{\partial x}\frac{\partial\delta\theta}{\partial x} + D_{xx}\frac{\partial\theta}{\partial x}\frac{\partial\delta\theta}{\partial x}) + \Big(1-(ea_0)^2\frac{\partial^2}{\partial x^2}\Big)(m_2\omega^2\theta\delta\theta - m_1\omega^2\varphi\delta\theta) + k_sA_{xz}(-\theta\frac{\partial\delta\psi}{\partial x} + \frac{\partial\psi}{\partial x}\frac{\partial\delta\psi}{\partial x}) + \Big(1-(ea_0)^2\frac{\partial^2}{\partial x^2}\Big)(m_0\omega^2\psi\delta\psi + k_w\psi\delta\psi + k_p\frac{\partial\psi}{\partial x}\frac{\partial\delta\psi}{\partial x} - A_{xx}^T\frac{\partial\psi}{\partial x}\frac{\partial\delta\psi}{\partial x})\Big]dx = 0. \tag{51}$$

Here, $\varphi_i(x)$, $\psi_i(x)$ and $\theta_i(x)$ are the shape functions. The axial displacement of a point that is not on the neutral axis is a linear function of both u and ϕ, therefore the degrees of the polynomials for $\varphi_i(x)$ and $\theta_i(x)$ have equal orders. Since the shear strain is a linear function of both the rotation ϕ and the slope of displacement, $\partial w/\partial x$, the degrees of the polynomials for $\psi_i(x)$ are one order higher than for $\varphi_i(x)$ and $\theta_i(x)$, in order to satisfy the compatibility conditions. Cubic polynomials for $\psi_i(x)$, and quadratic polynomials for $\varphi_i(x)$ and $\theta_i(x)$, are selected based on the Lagrange interpolation formula, and defined as [56]

$$[\varphi_1,\theta_1] = (1-\zeta)(1-2\zeta), \quad [\varphi_2,\theta_2] = 4\zeta(1-\zeta), \quad [\varphi_3,\theta_3] = -\zeta(1-2\zeta),$$
$$\psi_1 = (1-\zeta)\Big(1-\frac{3}{2}\zeta\Big)(1-3\zeta), \quad \psi_2 = 9\zeta(1-\zeta)\Big(1-\frac{3}{2}\zeta\Big), \quad \psi_3 = \frac{-9}{2}\zeta(1-\zeta)(1-3\zeta),$$
$$\psi_4 = \zeta(1-3\zeta)\Big(1-\frac{3}{2}\zeta\Big). \tag{52}$$

The equation of motion for a beam is given by

$$\boldsymbol{\bar{M}\ddot{U}} + (\boldsymbol{\bar{K}} - P\boldsymbol{\bar{K}_p})\boldsymbol{U} = \boldsymbol{0} \tag{53}$$

Here, $\boldsymbol{\bar{K}}$, $\boldsymbol{\bar{M}}$ and $\boldsymbol{\bar{K}_p}$ denote the global stiffness, mass and geometric stiffness matrices, respectively. $\boldsymbol{U}$ is the displacement vector. The following eigenvalue relation is deduced from Eq. (53) for free vibration investigations,

$$(\boldsymbol{\bar{K}} - \omega^2\boldsymbol{\bar{M}})\boldsymbol{U} = \boldsymbol{0} \tag{54}$$

Furthermore, for buckling analysis, by ignoring the time dependent terms in Eq. (53), the following equation is solved

$$(\boldsymbol{\bar{K}} - P_{cr}\boldsymbol{\bar{K}_p})\boldsymbol{U} = \boldsymbol{0} \tag{55}$$

In order to achieve the thermal buckling results for temperature dependent material properties, an iterative procedure is implemented as follows:

I. Calculate the material properties at the free stress temperature $T = T_0$.
II. Solve Eq. (51) and derive the critical buckling load ΔT_{cr}, which is the critical bucking load for temperature-independent material properties.
III. Update the temperature of the environment as $T = \Delta T_{cr} + T_0$, and obtain the new critical buckling temperature at T.

IV. Repeat step (III) to achieve a satisfactory error tolerance.

$$\varepsilon = \left|\frac{\Delta T_{cr}^{i+1} - \Delta T_{cr}^{i}}{\Delta T_{cr}^{i}}\right| \leq 0.1\% \quad (56)$$

The global matrices can be assembled in a standard procedure, by partitioning the element matrices based on the degrees of freedom of each end node, and the internal degrees of freedom, and given in the form

$$[\bar{\boldsymbol{K}}^{ij}] = \begin{bmatrix} k^{11} & 0 & k^{13} \\ 0 & k^{22} & k^{23} \\ k^{31} & k^{32} & k^{33} \end{bmatrix}, [\bar{\boldsymbol{K}}_P^{ij}] = \begin{bmatrix} 0 & 0 & 0 \\ 0 & k_p^{22} & 0 \\ 0 & 0 & 0 \end{bmatrix}, [\bar{\boldsymbol{M}}^{ij}] = \begin{bmatrix} m^{11} & 0 & m^{13} \\ 0 & m^{22} & 0 \\ m^{31} & 0 & m^{33} \end{bmatrix} \quad (57)$$

where

$k^{11} = A_{xx}k_{aa1}$, $k^{13} = -B_{xx}k_{aa1}$, $k^{23} = -A_{xz}k_{bc1}$, $k^{33} = k_s A_{xz}k_{aa} + D_{xx}k_{aa1}$,

$k^{22} = k_s A_{xz}k_{bb1}$, $m^{11} = m_0\omega^2 k_{aa} + (ea_0)^2 m_0\omega^2 k_{aa1}$, $m^{13} = -m_1\omega^2 k_{aa}(ea_0)^2 m_1\omega^2 k_{aa1}$,
$m^{33} = m_2\omega^2 k_{aa} + (ea_0)^2 m_2\omega^2 k_{aa1}$, $m^{22} = m_0\omega^2 k_{bb} + (ea_0)^2 m_0\omega^2 k_{bb1}$,
$k_p^{22} = -EA\alpha\Delta T(k_{bb1} + (ea_0)^2 k_{bb2})$. (58)

These matrices are explicitly defined in Appendix A.

3. Numerical results

The effects of P-FG material distribution, porosity, nonlocal effect, elastic foundation and thermal effect on the nondimensional natural frequencies and critical buckling temperature of P-FG nanobeams are examined in this section. The bottom surface of the P-FG nanobeam is pure steel ($SUS304$), and the top surface of the beam is pure ceramic (Si_3N_4), the corresponding material properties are given in Table 1. The following non-dimensional parameters are used in this section

$$\hat{\omega} = \omega L^2\sqrt{\frac{\rho_c A}{E_c I}}, \ \hat{P}_{cr} = \Delta T_{cr}\alpha_m\frac{L^2}{h^2}, K_w = \frac{k_w L^4}{E_c I}, K_p = \frac{k_p L^2}{E_c I} \quad (59)$$

where $\hat{\omega}$, $\hat{P}_{cr}$, K_w and K_p are related to the frequency, buckling parameter, the linear stiffness of the Winkler foundation and the shear stiffness corresponding to the Pasternak foundation. I is the second moment of inertia. The subscripts $()_m$ and $()_c$ denote the material properties of $SUS304$ and Si_3N_4 at ambient temperature, respectively.

3.2. Thermal buckling analysis

A convergence study is performed for the buckling behaviour of the proposed element. Figure 3 gives the critical buckling temperature of nonlocal FGM-II beams with different boundary conditions at $L/h = 20$, $k = 1$, $e_0 a/L = 0.1$, $\lambda = 0.3$, $K_w = 10$ and $K_p = 5$. This plot, shows that the results for the proposed element converge rapidly as the number of elements increases. Eight elements for pinned-pinned, and fifteen elements for fixed-pinned and fixed-fixed, boundary conditions are sufficient to achieve reasonable accuracy in the numerical calculations.

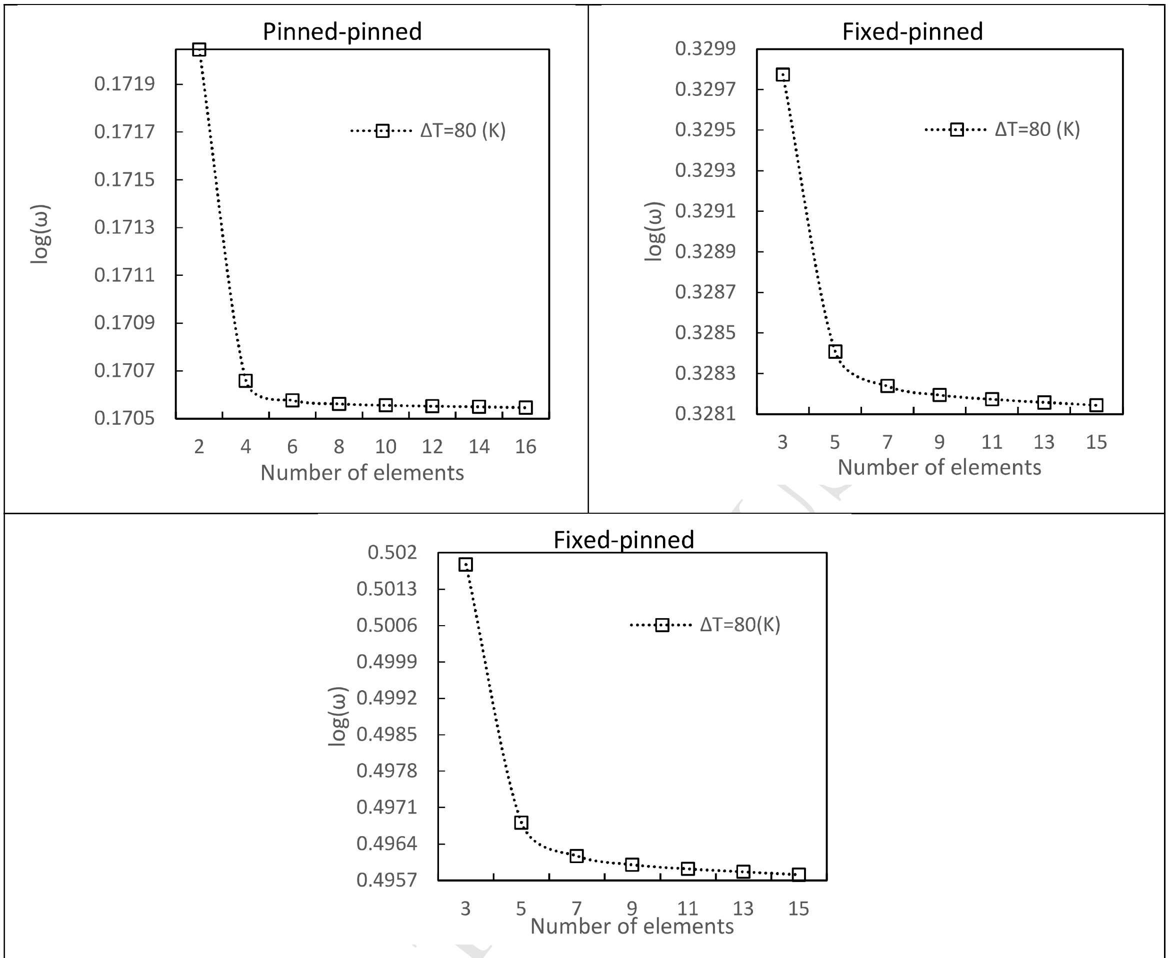

Fig. 3. Convergence rate of the proposed element for different boundary conditions ($L/h = 20$, $\Delta T = 80(K)$, $k = 1, K_w = 10, K_p = 5, e_0 a/L = 0.1, \lambda = 0.3$).

To validate the proposed model, the dimensionless thermal buckling parameter $\widehat{P}_{cr}$ for the proposed model is compared with those obtained by Wattanasakulpong et al. [57] in Table 2. In order to have an accurate comparison, the material properties are considered as Table 1 in both studies, and the thermal moment in the potential energy equation (Eq. 30) is ignored.

Table 2. Nondimensional thermal buckling $\hat{P}_{cr}$ of pinned-pinned beams with $L/h = 20$ for various material distributions.

Material	Present	Ref. [57]
Si_3N_4	1.154	1.185
k=0.2	0.990	0.991
k=0.5	0.870	0.882
k=1.0	0.786	0.805
k=2.0	0.731	0.749
k=5.0	0.690	0.697
k=10	0.665	0.664
$SUS304$	0.608	0.613

The variations of the nondimensional critical buckling parameter $\hat{P}_{cr}$ for pinned-pinned, fixed-pinned and fixed-fixed beam with different material distributions k, foundation stiffnesses (K_w, K_P), and porosity changes λ are given in Table 3 for FGM-I (uniformly distributed porosities) and FGM-II (functionally distributed porosities) nanobeams ($e_0a/l = 0.2$) with a span to depth ratio of $L/h = 20$. It is seen that for each porosity volume fraction, when the power law index k increases the nondimensional critical buckling reduces. When the power law index grows, the metal component turns out to be dominant in the material composition of the FG beam, and this situation results in a reduction in both the elasticity modulus and the transverse bending stiffness. Moreover, it is found that, as the porosity volume fraction grows, the nondimensional critical buckling parameter increases. It is noted that a P-FG beam with the functional distribution of porosities (FGM-II) is statically stable for lower thermal loadings, compared with a P-FG beam with uniformly distributed porosities (FGM-I).

Table 3. Nondimensional critical buckling parameter $\hat{P}_{cr}$ for FGM-I and FGM-II beams for pinned-pinned, fixed-pinned and fixed-fixed boundary conditions considering various material distributions k, elastic foundations (K_w, K_P) and porosity volume fractions λ. ($L/h = 20, e_0a/l = 0.2$).

k	(K_w, K_P)	Pinned-pinned						
		Perfect	FGM-I			FGM-II		
			$\lambda = 0.1$	$\lambda = 0.2$	$\lambda = 0.3$	$\lambda = 0.1$	$\lambda = 0.2$	$\lambda = 0.3$
0.1	(0,0)	1.0568	1.2047	1.4022	1.6615	1.1479	1.2537	1.3779
	(10,5)	1.6169	1.8814	2.2327	2.7117	1.7591	1.9222	2.1104
0.5	(0,0)	0.8676	0.9635	1.0834	1.2379	0.9335	1.0087	1.0951
	(10,5)	1.4035	1.6123	1.8646	2.2175	1.5197	1.6528	1.7877
1	(0,0)	0.7837	0.8598	0.952	1.0655	0.8398	0.9035	0.9761

	(10,5)	1.3033	1.4875	1.7263	2.025	1.4078	1.5269	1.6638
5	(0,0)	0.6885	0.748	0.8188	0.9044	0.7355	0.7897	0.8518
	(10,5)	1.1967	1.3652	1.5879	1.8991	1.2925	1.4036	1.5327
k	(K_w, K_P)	Fixed-pinned						
		Perfect	FGM-I			FGM-II		
			$\lambda = 0.1$	$\lambda = 0.2$	$\lambda = 0.3$	$\lambda = 0.1$	$\lambda = 0.2$	$\lambda = 0.3$
0.1	(0,0)	1.9151	2.1557	2.4666	2.9301	2.063	2.231	2.4225
	(10,5)	2.377	2.7046	3.1852	3.8128	2.5616	2.7691	3.0573
0.5	(0,0)	1.5999	1.7615	1.9588	2.2038	1.7109	1.8357	1.9765
	(10,5)	2.048	2.2969	2.6084	3.0517	2.1967	2.3637	2.5516
1	(0,0)	1.4687	1.6043	1.7458	1.9323	1.5683	1.6637	1.7857
	(10,5)	1.9023	2.1222	2.3967	2.7455	2.0377	2.1902	2.3627
5	(0,0)	1.3001	1.4082	1.5368	1.6922	1.3866	1.4846	1.5966
	(10,5)	1.7545	1.9625	2.2335	2.6133	1.8854	2.0359	2.2112
k	(K_w, K_P)	Fixed-fixed						
		Perfect	FGM-I			FGM-II		
			$\lambda = 0.1$	$\lambda = 0.2$	$\lambda = 0.3$	$\lambda = 0.1$	$\lambda = 0.2$	$\lambda = 0.3$
0.1	(0,0)	3.2194	3.6016	4.1024	4.627	3.4515	3.7171	3.9385
	(10,5)	3.6099	4.0707	4.5453	5.4028	3.8754	4.0971	4.3921
0.5	(0,0)	2.6705	2.96	3.2695	3.5247	2.8811	3.0752	3.2967
	(10,5)	3.0913	3.4185	3.7428	4.187	3.2963	3.5285	3.7116
1	(0,0)	2.4584	2.6857	2.9241	3.1128	2.5974	2.8014	2.9905
	(10,5)	2.8327	3.1456	3.4925	3.7828	3.0507	3.2567	3.4928
5	(0,0)	2.2438	2.4172	2.6193	2.8479	2.384	2.5432	2.7259
	(10,5)	2.6632	2.9641	3.3261	3.8336	2.8752	3.0926	3.3525

The variations of critical buckling temperature ΔT_{cr}, with span to depth ratio L/h, are plotted in Fig. 4 for perfect, FGM-I and FGM-II nanobeams ($e_0 a/L = 0.2$) with various boundary conditions and power index of $k = 1$. The critical temperature decreases as the span to depth ratio increases, and this variation happens quickly at smaller slenderness ratios. It is observed that the FGM-I nanobeam has higher critical buckling temperatures in comparison with perfect and FGM-II nanobeams. The influence of the functional distribution of porosities (FGM-II) on the critical buckling temperature is not so significant (especially for the pinned-pinned boundary conditions), although the critical buckling temperature is influenced significantly by the uniform distribution of porosities (FGM-I). Also, for high span to depth ratios the critical temperatures for all three beams (perfect, FGM-I and FGM-II) converge to a unique value, which happens at a higher rate for the pinned-pinned boundary conditions.

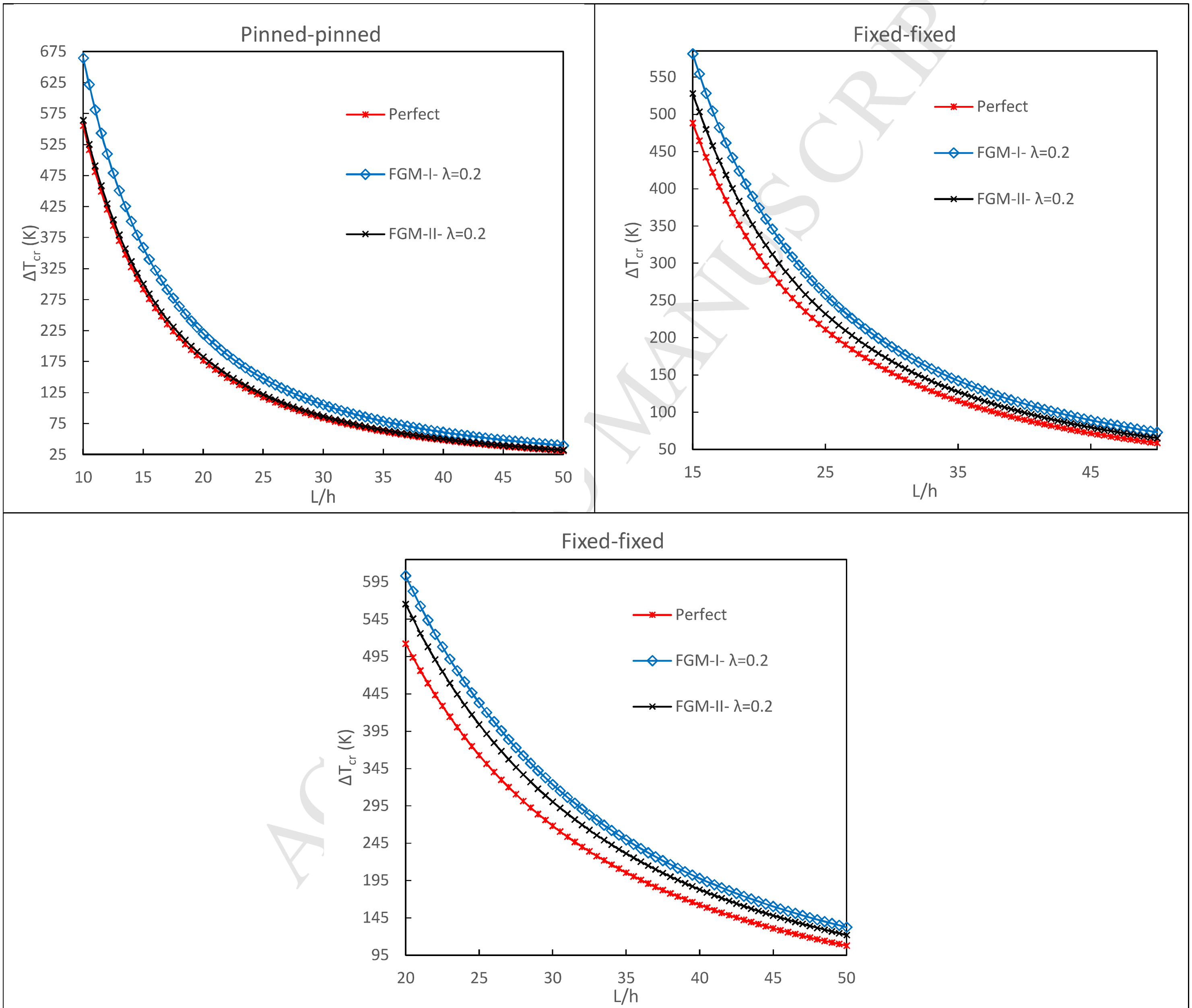

Fig. 4. Critical buckling temperature ΔT_{cr} for perfect, FGM-I and FGM-II nanobeams with pinned-pinned, fixed-pinned and fixed-fixed boundary conditions ($e_0a/L = 0.2$, $k = 1$).

3.2. Thermal vibration analysis

A convergence study is performed for vibration behaviour of the proposed element. Figure 5 shows the nondimensional fundamental frequencies of nonlocal P-FG beams with different boundary conditions for $L/h = 20$, $e_0a/L = 0.1$, $K_w = 10, K_p = 5$ and $k = 1$ at $\Delta T = 80$. The frequencies predicted by the proposed element converge rapidly as the number of elements increase. Eight elements should to be enough to obtain reasonable accuracy in numerical calculations.

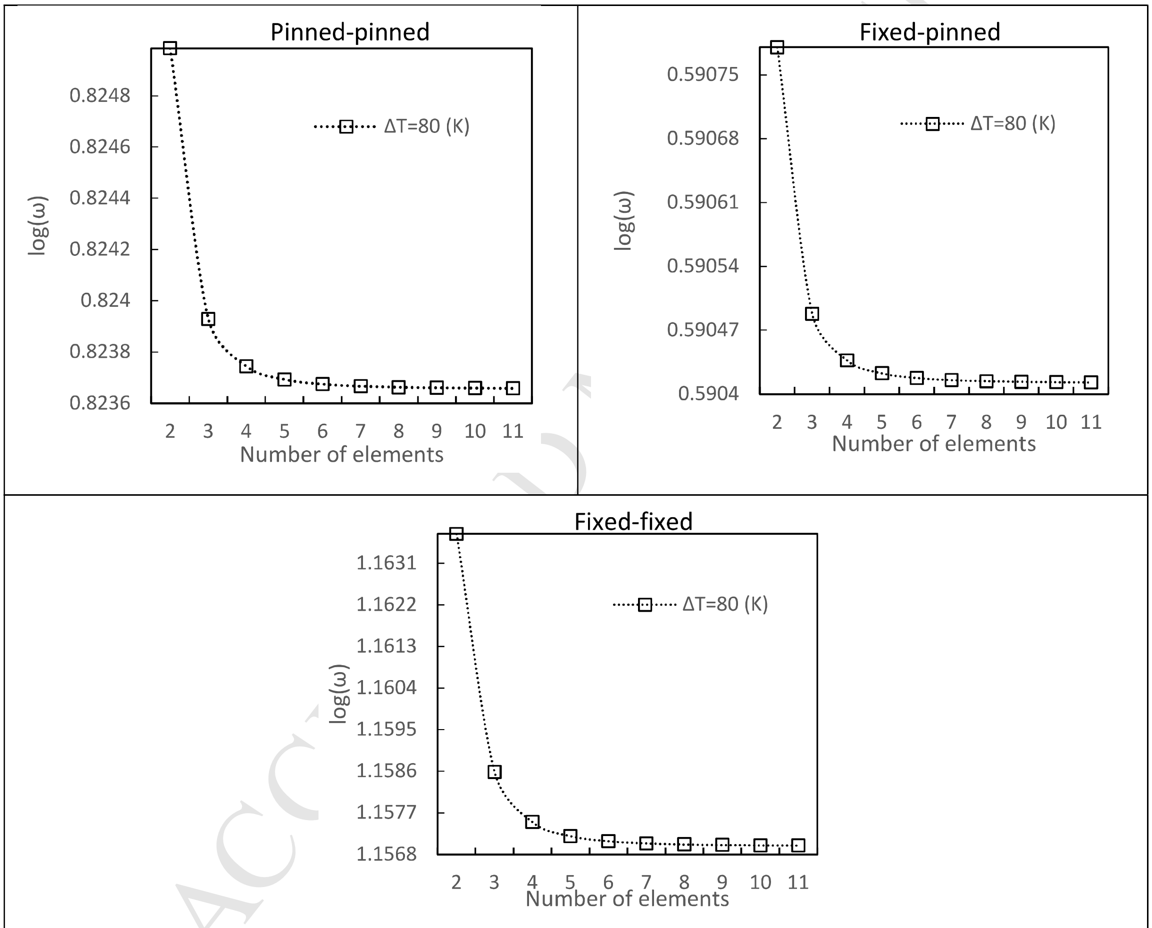

Fig. 5. Convergence rate of the proposed element for different boundary conditions ($L/h = 20, \Delta T = 80,\ k = 1, K_w = 10, K_p = 5, e_0a/L = 0.1$).

The reliability of the vibration response for the proposed FE model can be concluded from Table 4, where the nondimensional natural frequencies of the FG nonlocal Timoshenko beam on the

Winkler-Pasternak foundation with thermal loading, are given and compared to the analytical solution of Ebrahimi and Barati [58].

Table 4. Comparison of the non-dimensional frequency $\widehat{\omega}$ of an FGM-I nanobeam on elastic foundation for pinned-pinned boundary conditions with different temperature variations ΔT, elastic stiffnesses (K_w, K_p) and nonlocal parameters e_0a/L $(L/h = 20,\ k = 1)$.

e_0a/L	(K_w, K_p)	$\Delta T(K)$	Present	Ref. [58]	Error
0	(0,0)	20	5.58038	5.56965	0.19%
		40	5.19787	5.20291	-0.09%
	(25,10)	20	9.29645	9.30304	-0.07%
		40	9.05918	9.08822	-0.32%
1	(0,0)	20	5.28998	5.28078	0.17%
		40	4.88365	4.89213	-0.17%
	(25,10)	20	9.09377	9.13302	-0.43%
		40	8.85757	8.91395	-0.63%

The variations of the nondimensional fundamental frequency $\widehat{\omega}$ for pinned-pinned, fixed-pinned and fixed-fixed beams with various material distributions k, foundation stiffnesses (K_w, K_P), temperature changes ΔT and nonlocal parameters e_0a/l are given in Tables 5 and 6 for FGM-I, and FGM-II beams, respectively. It is found that for each kind of thermo-mechanical loading, when the power law index k grows, the nondimensional frequency decreases. As the nonlocal parameter increases the nondimensional frequency reduces and the nonlocal parameter has a softening effect on the natural frequency of both FGM-I and FGM-II beams even with a small increment of the nonlocal parameter. Also, the foundation parameters have an increasing effect on the nondimensional frequencies by providing a greater stiffness to the whole system. For example, at $e_0a/L = 0.2$, $\Delta T = 40(K)$ and $k = 5$, for pinned-pinned boundary conditions, when the foundation stiffness increases from (0,0) to (10,5), the nondimensional frequency of FGM-I and FGM-II nanobeams increases by 41% and 39%, respectively. Furthermore, the functional distribution of porosities (FGM-II) results in a smaller frequency in comparison with a uniform distribution of porosities (FGM-I).

Table 5. Nondimensional natural frequency $\widehat{\omega}$ of FGM-I for pinned-pinned, fixed-pinned and fixed-fixed boundary conditions considering various material distributions k,elastic foundations (K_w, K_P) and nonlocal parameters e_0a/l. $(L/h = 20, \lambda = 0.1)$.

Pinned-pinned			
k	(K_w, K_P)	$e_0a/L = 0$	$e_0a/L = 0.2$

		$\Delta T(K)$			$\Delta T(K)$		
		0	20	40	0	20	40
0.1	(0,0)	9.1985	8.8498	8.4803	9.109	8.7571	8.3839
	(10,5)	11.9928	11.7167	11.4293	11.9231	11.6458	11.3573
0.5	(0,0)	16.0649	15.3908	14.6719	15.9086	15.2282	14.5018
	(10,5)	21.1753	20.6494	20.1006	21.0545	20.5267	19.9755
1	(0,0)	21.9855	20.997	19.9379	21.7716	20.7737	19.7031
	(10,5)	29.2158	28.4532	27.6554	29.0516	28.2861	27.4849
5	(0,0)	26.7267	25.4427	24.0593	26.4667	25.1702	23.7715
	(10,5)	35.8124	34.8336	33.8071	35.6139	34.6315	33.6008
Fixed-pinned							
k	(K_w, K_P)	e_0a/L=0			e_0a/L=0.2		
		$\Delta T(K)$			$\Delta T(K)$		
		0	20	40	0	20	40
0.1	(0,0)	14.2943	14.0204	13.7364	14.1328	13.8519	13.5602
	(10,5)	16.4677	16.2238	15.9724	16.3575	16.1089	15.8526
0.5	(0,0)	24.9724	24.4482	23.9023	24.6902	24.1522	23.5911
	(10,5)	28.9563	28.494	28.0158	28.7675	28.2962	27.8084
1	(0,0)	34.1845	33.421	32.6233	33.7983	33.0142	32.1939
	(10,5)	39.8305	39.1617	38.4683	39.5759	38.894	38.1866
5	(0,0)	41.5546	40.5688	39.5351	41.0852	40.0724	39.0088
	(10,5)	48.6637	47.8066	46.9159	48.3588	47.4849	46.5761
Fixed-fixed							
k	(K_w, K_P)	e_0a/L=0			e_0a/L=0.2		
		$\Delta T(K)$			$\Delta T(K)$		
		0	20	40	0	20	40
0.1	(0,0)	20.6045	20.3824	20.155	20.3564	20.1227	19.8829
	(10,5)	22.2486	22.0375	21.822	22.0899	21.8697	21.6445
0.5	(0,0)	35.9858	35.5668	35.1356	35.5524	35.1105	34.6551
	(10,5)	39.0055	38.6095	38.2032	38.7355	38.3219	37.897

1	(0,0)	49.2459	48.6412	48.0169	48.6528	48.0143	47.354
	(10,5)	53.532	52.9628	52.3771	53.17	52.575	51.9619
5	(0,0)	59.8529	59.0788	58.2768	59.1323	58.3139	57.4646
	(10,5)	65.2574	64.532	63.7833	64.8265	64.0678	63.2836

Table 6. Nondimensional natural frequency $\widehat{\omega}$ of FGM-II for pinned-pinned, fixed-pinned and fixed-fixed boundary conditions considering various material distributions k,elastic foundations (K_w, K_P) and nonlocal parameters e_0a/l. $(L/h = 20, \lambda = 0.1)$.

Pinned-pinned							
k	(K_w, K_P)	$e_0a/L = 0$			$e_0a/L = 0.2$		
		$\Delta T(K)$			$\Delta T(K)$		
		0	20	40	0	20	40
0.1	(0,0)	9.0273	8.666	8.2822	8.9395	8.5749	8.1871
	(10,5)	11.6095	11.3208	11.0196	11.5402	11.2503	10.9477
0.5	(0,0)	15.9251	15.2242	14.4749	15.7702	15.0626	14.3053
	(10,5)	20.6828	20.1301	19.5518	20.5615	20.0066	19.4256
1	(0,0)	21.9296	20.9001	19.7944	21.7164	20.6769	19.5591
	(10,5)	28.6886	27.8847	27.0417	28.5226	27.7154	26.8686
5	(0,0)	26.795	25.456	24.0106	26.5344	25.1824	23.7207
	(10,5)	35.3149	34.2805	33.1932	35.1132	34.0746	32.9824
Fixed-pinned							
k	(K_w, K_P)	e_0a/L=0			e_0a/L=0.2		
		$\Delta T(K)$			$\Delta T(K)$		
		0	20	40	0	20	40
0.1	(0,0)	14.0256	13.743	13.4495	13.8671	13.5772	13.2757
	(10,5)	16.0278	15.775	15.514	15.9169	15.6591	15.3928
0.5	(0,0)	24.7493	24.2061	23.6394	24.4698	23.912	23.3294
	(10,5)	28.4461	27.9641	27.4649	28.2537	27.7621	27.2526
1	(0,0)	34.0884	33.2952	32.4654	33.7034	32.8887	32.0351
	(10,5)	39.348	38.6486	37.9225	39.0864	38.373	37.6317
5	(0,0)	41.6488	40.6228	39.546	41.1785	40.1242	39.0161

	(10,5)	48.2908	47.392	46.4568	47.9752	47.0585	46.1038
Fixed-fixed							
k	(K_w, K_P)	e_0a/L=0			e_0a/L=0.2		
		$\Delta T(K)$			$\Delta T(K)$		
		0	20	40	0	20	40
0.1	(0,0)	20.2127	19.985	19.7514	19.9694	19.7296	19.4831
	(10,5)	21.7244	21.5076	21.2859	21.5636	21.3372	21.1053
0.5	(0,0)	35.6574	35.2251	34.7797	35.2282	34.772	34.3013
	(10,5)	38.4534	38.0439	37.6233	38.176	37.7478	37.3075
1	(0,0)	49.099	48.4731	47.8263	48.508	47.8468	47.1624
	(10,5)	53.0825	52.4917	51.8832	52.707	52.0889	51.4513
5	(0,0)	59.9783	59.1749	58.3422	59.2566	58.407	57.5248
	(10,5)	65.015	64.2598	63.4796	64.5644	63.7738	62.956

In Fig. 6 the fundamental frequency of an FG nanobeam on an elastic foundation is plotted for different boundary conditions with respect to the temperature variations and various Winkler-Pasternak foundation parameters. The compressive axial forces caused by the thermal loads created from the temperature changes can make the beam statically unstable by passing the critical value. The temperature rise essentially softens the stiffness of the beam, which results in the reduction of the nondimensional frequency. This trend continues until the critical temperature is reached. Also the existence of the elastic foundation provides more rigidity to the system, which increases the nondimensional frequency. This behaviour also occurs until the critical temperature is reached. Moreover, based on Fig. 6, by comparing the frequency changes before the critical point, it is found that the shear stiffness (Pasternak foundation) of the foundation gives more bending rigidity to the system than the linear stiffness (Winkler foundation). Furthermore, as expected, the critical temperature is distinct for each of the boundary conditions, for example, considering the foundation with $K_w = 30$ and $K_P = 15$ values of foundation stiffness, the critical temperature will be 89.3K, 114.24K and 161.14K for pinned-pinned, fixed-pinned and fixed-fixed boundary conditions, respectively.

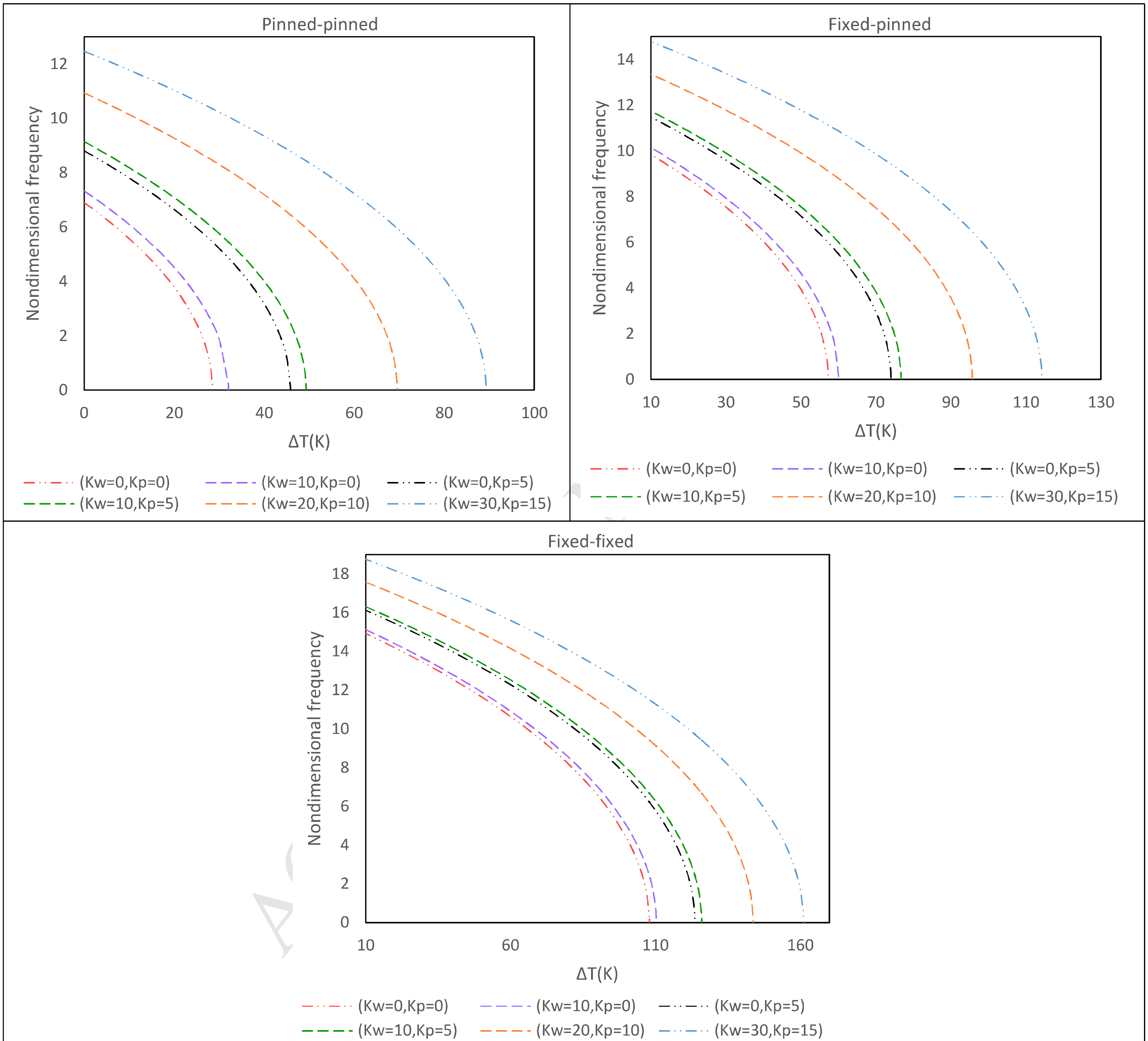

Fig. 6. Influence of the Winkler-Pasternak elastic foundation on the nondimensional frequency of the FGM-I nanobeam with respect to temperature rise for different boundary conditions ($k = 1, L/h = 50, e_0 a/L = 0.2, \lambda = 0.1$).

The effect of the material graduation k and span-depth ratio L/h on the nondimensional frequency of the FGM-I and FGM-II porous ($\lambda = 0.1$) nanobeams ($e_0a/L = 0.2$) resting on an elastic foundation ($K_w = 300, K_P = 150$) and made of $Si_3N_4/SUS304$ are shown in Fig. 7 for different boundary conditions and temperature rises. The functional distribution of porosities (FGM-II) leads to a lower frequency in comparison with the uniform distribution of porosities (FGM-I), which is caused by the reduction of the stiffness of the P-FG beam. Also, considering the $L/h = 150$ beam, both types of PFGMs (FGM-I and FGM-II), reach their critical point at the ceramic dominant region. Specifically, the FGM-II beam attains the critical point in a more ceramic dominant area where for the fixed-pinned beam, with $k = 0.09$, the FG beam can almost be considered as a pure ceramic beam. For $L/h = 150$ nanobeams with pinned-pinned boundary conditions and a temperature rise of $\Delta T = 90$, the nondimensional natural frequencies decrease to zero at $k = 0.775$ and $k = 0.193$ for the FGM-I and FGM-II nanobeams, respectively. Meanwhile, this temperature rise is much less than the critical temperature for $L/h = 100$ and $L/h = 50$ nanobeams. This means that the nondimensional frequencies regarding these two nanobeams will never reach zero at $\Delta T = 90$. For fixed-pinned nanobeams with span to depth ratios of $L/h = 150$, the critical buckling temperature is $\Delta T = 95$, which occurs at $k = 0.412$ and $k = 0.09$ material graduations for the FGM-I and FGM-II nanobeams, respectively. Furthermore, for fixed-fixed nanobeams, the corresponding critical temperature of $L/h = 150$ is $\Delta T = 100$, which happens at $k = 0.508$ and $k = 0.15$ material distributions, for the FGM-I and FGM-II nanobeams, respectively.

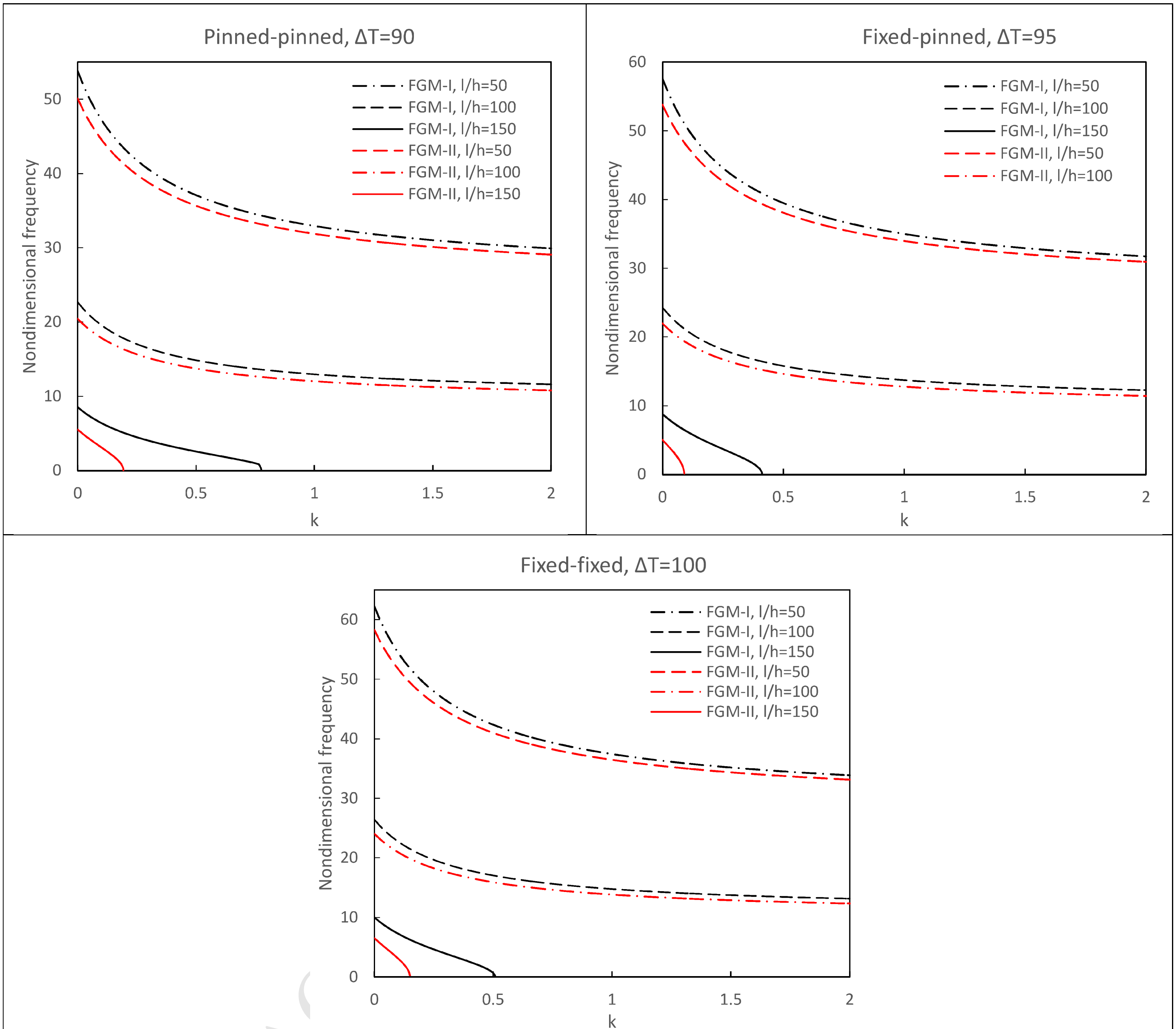

Fig. 7. Influence of the material distribution k and span-depth ratio L/h on the nondimensional frequency of the FGM-I and FGM-II nanobeams for different boundary conditions ($e_0a/L = 0.2, \lambda = 0.1, K_w = 300, K_P = 150$).

The variations of the nondimensional frequencies of FGM-I and FGM-II nanobeams ($e_0a/L = 0.2$) on elastic foundations ($K_w = 10, K_P = 5$), with material graduation k in the range $0 < k < 2$ for various thermal loadings are plotted in Fig. 8 for pinned-pinned boundary conditions. The closest result to the perfect FGM is the P-FGM with a functional distribution of the porosities

(FGM-II), which reaches to the critical buckling point right after the perfect FG beam. At $\Delta T = 140$, the nondimensional frequency related to the perfect FG beam, declines sharply as the value of the material graduation k grows until reaching the critical value at $k = 0.493$. This means that, for a perfect FG beam with the material distribution of $k = 0.493$ and pinned-pinned boundary conditions , $\Delta T = 140$ is the critical buckling temperature. $\Delta T = 140$ is also the critical temperature for FGM-II with porosity volume fraction of λ=0.1 at $k = 1.088$. With the considered domain for the material graduation k, there are three critical points for the temperature rise of $\Delta T = 145$, at $k = 0.36$, $k = 0.767$ and $k = 1.451$, for perfect FGM, FGM-II- λ=0.1 and FGM-I- λ=0.1, respectively. By increasing the thermal loading to $\Delta T = 150$, another critical point appears. At this temperature difference, the corresponding critical points are $k = 0.26$, $k = 0.565$, $k = 1.003$ and $k = 1.302$, for perfect FGM, FGM-II- λ=0.1, FGM-I- λ=0.1 and FGM-II- λ=0.2, respectively. At $\Delta T = 155$, the diagrams shift to the left and the critical points are $k = 0.184$, $k = 0.425$, k=0.741 and $k = 0.917$, for perfect FGM, FGM-II- λ=0.1, FGM-I- λ=0.1 and FGM-II- λ=0.2, respectively. This vibration behaviour is also investigated for fixed-pinned and fixed-fixed boundary conditions and the results are shown in Figs. 9 and 10, respectively. As expected, the bucking occurs at higher temperatures for these two boundary conditions in comparison with pinned-pinned boundary conditions.

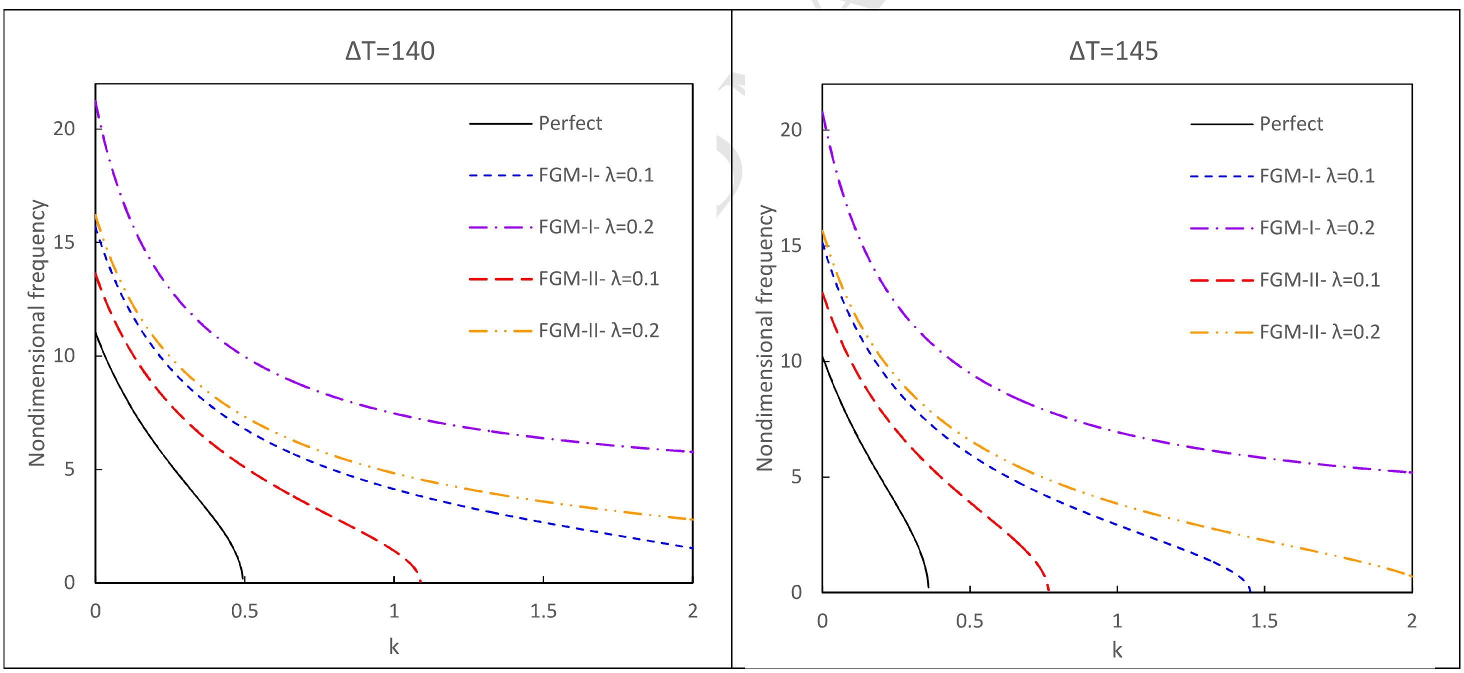

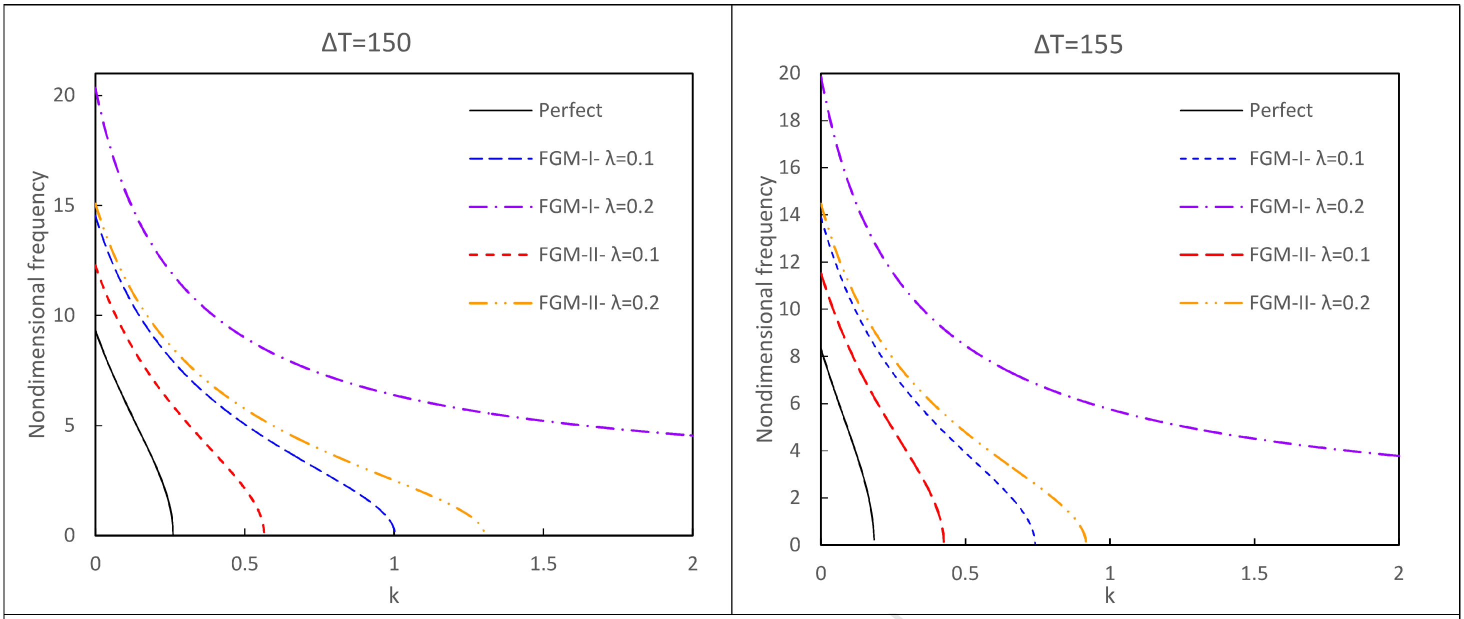

Fig. 8. Influence of the material distribution k and porosity on the nondimensional frequency of the FGM-I and FGM-II nanobeams with different thermal loadings for pinned-pinned boundary conditions ($e_0a/L = 0.2, K_w = 10, K_P = 5$).

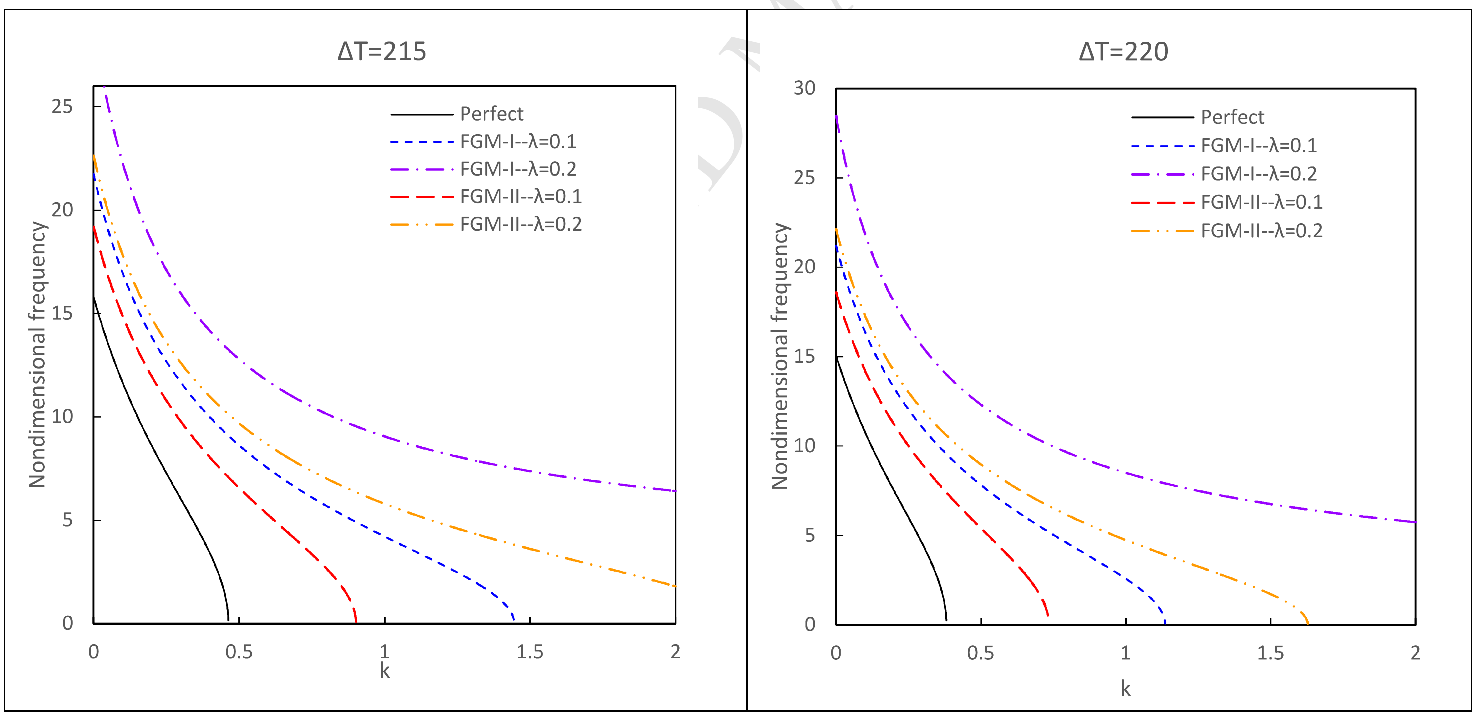

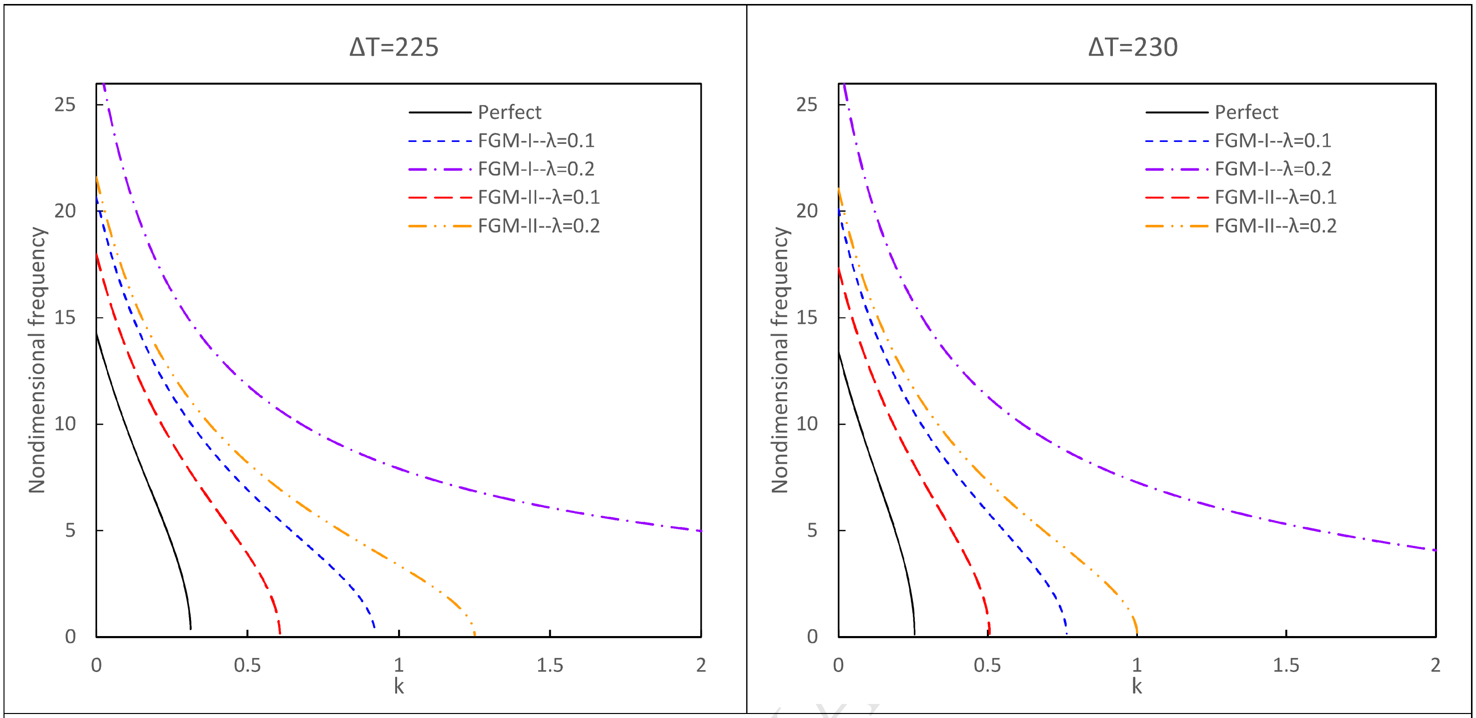

Fig. 9. Influence of the material distribution k and porosity on the nondimensional frequency of the FGM-I and FGM-II nanobeams with different thermal loadings for fixed-pinned boundary conditions ($e_0a/L = 0.2, K_w = 10, K_P = 5$).

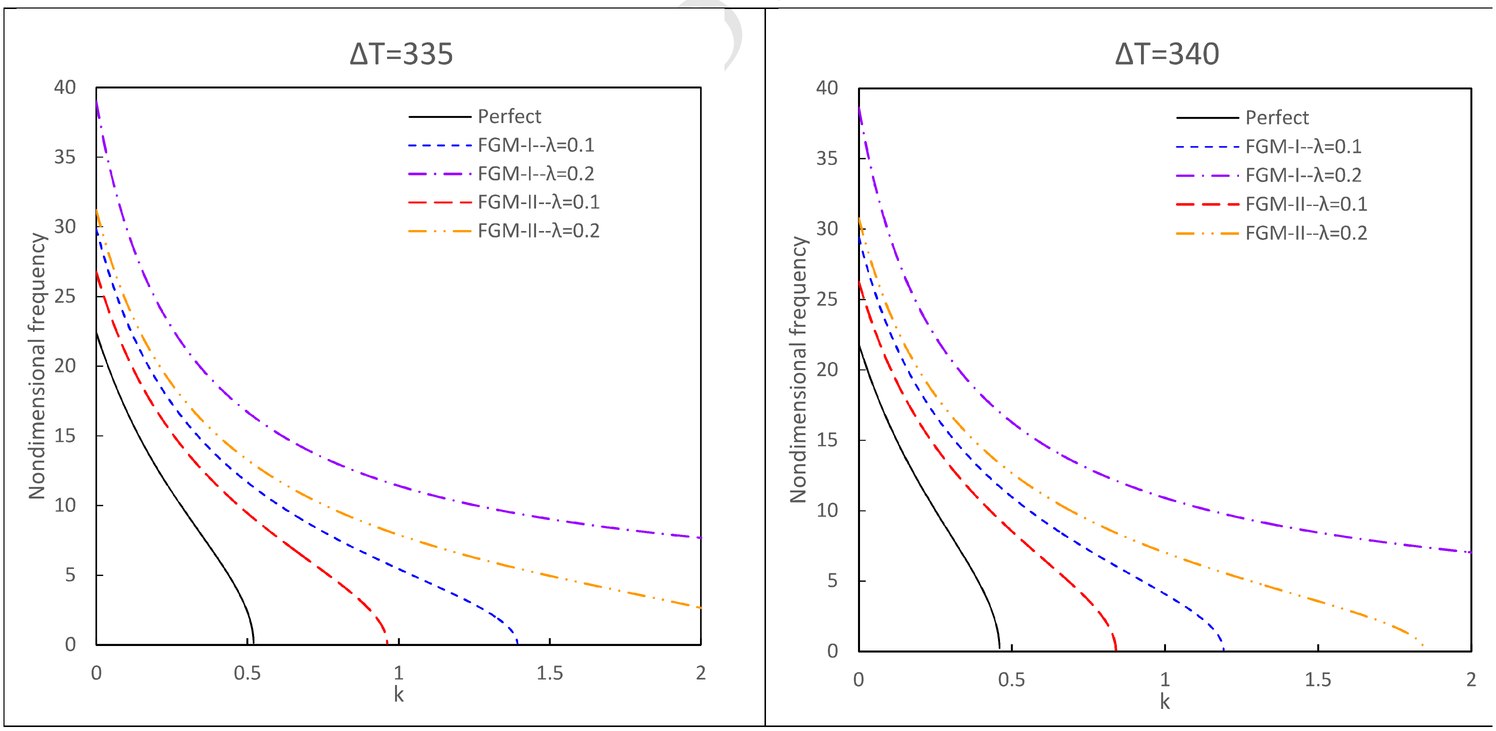

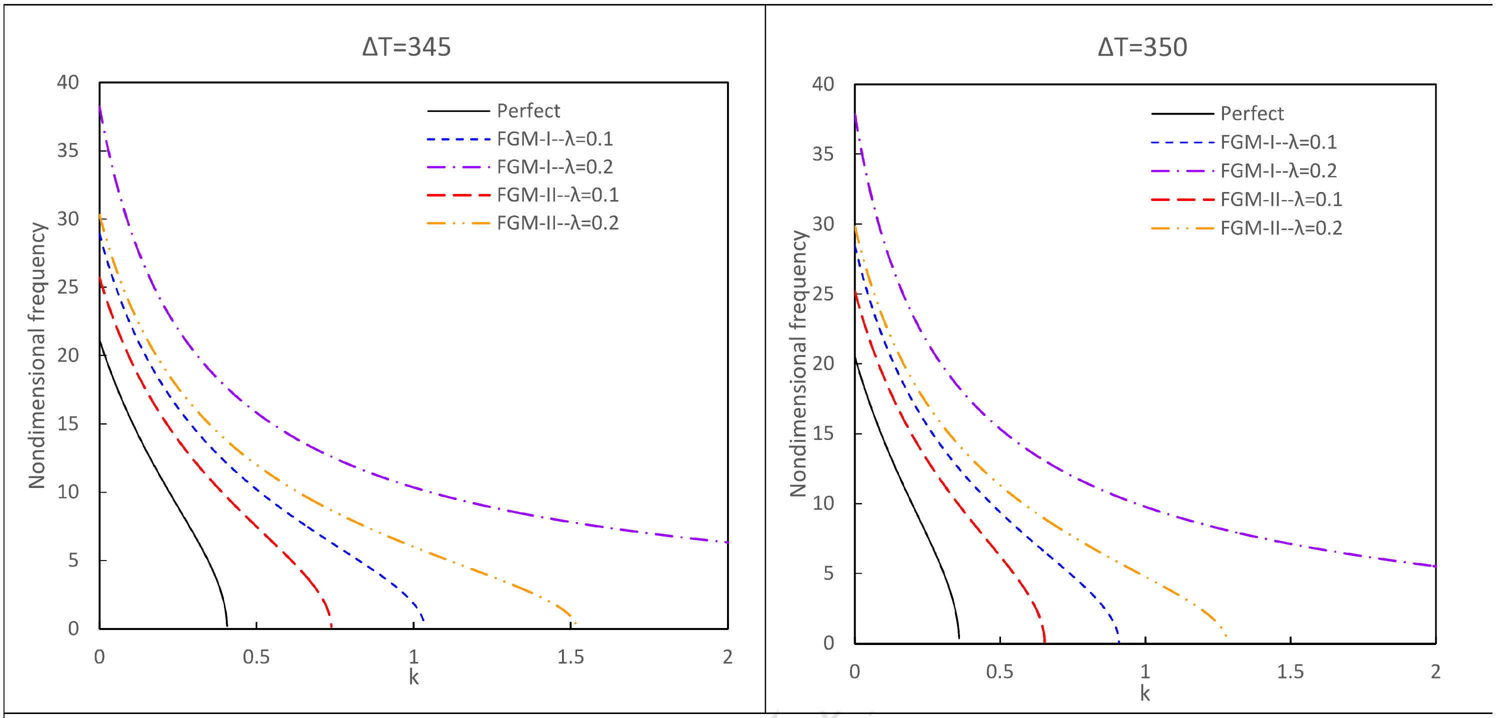

Fig. 10. Influence of the material distribution k and porosity on the nondimensional frequency of the FGM-I and FGM-II nanobeams with different thermal loadings for fixed-fixed boundary conditions ($e_0a/L = 0.2, K_w = 10, K_P = 5$).

4. Conclusion

A five noded beam element is proposed to study the thermo-elastic behaviour of temperature-dependent P-FG Timoshenko nanobeams subjected to a uniform temperature gradient through the thickness direction in the framework of nonlocal elasticity theory. In order to incorporate the size effects, Eringen's nonlocal elasticity theory is employed. The governing equations and the corresponding boundary conditions are deduced by exploiting Hamilton's principle. Verification of the proposed model is evaluated by comparing the results with the available data in the literature. The influences of two kinds of porosity distributions related to the FGM-I and FGM-II beams, the nonlocal scale parameter, material distribution, temperature gradient, foundation stiffness and slenderness ratio on the critical buckling temperature and natural frequencies of P-FG nanobeams are analysed. It is concluded that that presence of porosity leads to increases in the natural frequency. Also, it is seen that the functional distribution of the porosities results in smaller fundamental frequencies, in comparison with the uniform distribution of the porosities. The natural frequency reduces with an increase in the temperature and reaches zero at the critical temperature. This reduction in natural frequency with increasing temperature is related to the compressive stress caused by the thermal stress, which softens the beam stiffness. Based on the results of this paper, the existence of porosities increases the critical buckling temperature. Also, the uniform distribution of porosities (FGM-I) leads to higher buckling temperatures compared with the functional distribution of porosities (FGM-II), which could be considered as a critical factor in the optimisation and design of the porous functionally graded nanobeams.

Appendix A

$$k_{aa} = \frac{L}{15}\begin{bmatrix} 2 & 1 & -1/2 \\ 1 & 8 & 1 \\ -1/2 & 1 & 2 \end{bmatrix}, \tag{A1}$$

$$k_{aa1} = \frac{1}{3L}\begin{bmatrix} 7 & -8 & 1 \\ -8 & 16 & -8 \\ 1 & -8 & 7 \end{bmatrix}, \tag{A2}$$

$$k_{aa2} = \frac{16}{L^3}\begin{bmatrix} 1 & -2 & 1 \\ -2 & 4 & -2 \\ 1 & -2 & 1 \end{bmatrix}, \tag{A3}$$

$$k_{bb} = \frac{L}{1680}\begin{bmatrix} 128 & 99 & -36 & 19 \\ 99 & 648 & -81 & -36 \\ -36 & -81 & 648 & 99 \\ 19 & -36 & 99 & 128 \end{bmatrix}, \tag{A4}$$

$$k_{bb1} = \frac{1}{40L}\begin{bmatrix} 148 & -189 & 54 & -13 \\ -189 & 432 & -297 & 54 \\ 54 & -297 & 432 & -189 \\ -13 & 54 & -189 & 148 \end{bmatrix}, \tag{A5}$$

$$k_{bb2} = \frac{81}{L^3}\begin{bmatrix} 1 & -5/2 & 2 & -1/2 \\ -5/2 & 7 & -13/2 & 2 \\ 2 & -13/2 & 7 & -5/2 \\ -1/2 & 2 & -5/2 & 1 \end{bmatrix}, \tag{A6}$$

$$k_{bc1} = \frac{1}{120}\begin{bmatrix} -83 & -44 & 7 \\ 99 & -108 & 9 \\ -9 & 108 & -99 \\ -7 & 44 & 83 \end{bmatrix}, \tag{A7}$$

$$k_{bc2} = \frac{1}{2L^2}\begin{bmatrix} -27 & 18 & -9 \\ 63 & -54 & 45 \\ -45 & 54 & -63 \\ 9 & -18 & 27 \end{bmatrix}, \tag{A8}$$

where L is length of the beam element.

Data Availability

All of the results given in the paper are simulated based on the proposed finite element model. The paper contains full details of the developed finite element and the geometry and material properties for the examples. Hence, there is no raw data, and data in the figures and tables maybe be reproduced by coding the described model.

References

1. Koizumi M., 1993. The concept of FGM, Ceramic transactions. Functionally Gradient Materials. 34, pp.3-10.
2. Koizumi, M.F.G.M., 1997. FGM activities in Japan. Composites Part B: Engineering, 28(1-2), pp.1-4.
3. Shahverdi, H. and Barati, M.R., 2017. Vibration analysis of porous functionally graded nanoplates. International Journal of Engineering Science, 120, pp.82-99.
4. Aria, A.I. and Biglari, H., 2018. Computational vibration and buckling analysis of microtubule bundles based on nonlocal strain gradient theory. Applied Mathematics and Computation, 321, pp.313-332.
5. Friswell, M.I., Adhikari, S. and Lei, Y., 2007. Vibration analysis of beams with nonlocal mediums using the finite element method. International Journal for Numerical Methods in Engineering, 71(11), pp.1365-1386.
6. Phadikar, J.K. and Pradhan, S.C., 2010. Variational formulation and finite element analysis for nonlocal elastic nanobeams and nanoplates. Computational materials science, 49(3), pp.492-499.
7. Murmu, T. and Adhikari, S., 2010. Nonlocal transverse vibration of double-nanobeam-systems. Journal of Applied Physics, 108(8), p.083514.
8. Roque, C.M.C., Ferreira, A.J.M. and Reddy, J.N., 2011. Analysis of Timoshenko nanobeams with a nonlocal formulation and meshless method. International Journal of Engineering Science, 49(9), pp.976-984.
9. Wu, C.P. and Li, W.C., 2016. Three-Dimensional Static Analysis of Nanoplates and Graphene Sheets by Using Eringen's Nonlocal Elasticity Theory and the Perturbation Method. CMC-COMPUTERS MATERIALS & CONTINUA, 52(2), pp.73-103.
10. Eringen, A.C., 1983. On differential equations of nonlocal elasticity and solutions of screw dislocation and surface waves. Journal of applied physics, 54(9), pp.4703-4710.
11. Mirjavadi, S.S., Afshari, B.M., Barati, M.R. and Hamouda, A.M.S., 2019. Transient response of porous FG nanoplates subjected to various pulse loads based on nonlocal stress-strain gradient theory. European Journal of Mechanics-A/Solids, 74, pp.210-220.
12. Shahrbabaki, E.A., 2018. On three-dimensional nonlocal elasticity: Free vibration of rectangular nanoplate. European Journal of Mechanics-A/Solids, 71, pp.122-133.
13. Nguyen, N.T., Kim, N.I. and Lee, J., 2015. Mixed finite element analysis of nonlocal Euler–Bernoulli nanobeams. Finite Elements in Analysis and Design, 106, pp.65-72.
14. Lei, Y., Adhikari, S. and Friswell, M.I., 2013. Vibration of nonlocal Kelvin–Voigt viscoelastic damped Timoshenko beams. International Journal of Engineering Science, 66, pp.1-13.

15. Barretta, R., Luciano, R., de Sciarra, F.M. and Ruta, G., 2018. Stress-driven nonlocal integral model for Timoshenko elastic nano-beams. European Journal of Mechanics-A/Solids.
16. Arefi, M., 2018. Analysis of a doubly curved piezoelectric nano shell: Nonlocal electro-elastic bending solution. European Journal of Mechanics-A/Solids, 70, pp.226-237.
17. Xia, W., Feng, Y.P. and Zhao, D.W., 2015. Finite element multi-mode approach to thermal postbuckling of functionally graded plates. Computers, Materials, & Continua, 46(2), pp.125-144.
18. Challamel, N., Aydogdu, M. and Elishakoff, I., 2018. Statics and dynamics of nanorods embedded in an elastic medium: Nonlocal elasticity and lattice formulations. European Journal of Mechanics-A/Solids, 67, pp.254-271.
19. Daneshmehr, A. and Rajabpoor, A., 2014. Stability of size dependent functionally graded nanoplate based on nonlocal elasticity and higher order plate theories and different boundary conditions. International Journal of Engineering Science, 82, pp.84-100.
20. Nami, M.R. and Janghorban, M., 2014. Resonance behaviour of FG rectangular micro/nano plate based on nonlocal elasticity theory and strain gradient theory with one gradient constant. Composite Structures, 111, pp.349-353.
21. Rahmani, O. and Pedram, O., 2014. Analysis and modelling the size effect on vibration of functionally graded nanobeams based on nonlocal Timoshenko beam theory. International Journal of Engineering Science, 77, pp.55-70.
22. Ebrahimi, F. and Salari, E., 2015. Thermal buckling and free vibration analysis of size dependent Timoshenko FG nanobeams in thermal environments. Composite Structures, 128, pp.363-380.
23. Ebrahimi, F. and Salari, E., 2015. Size-dependent free flexural vibrational behaviour of functionally graded nanobeams using semi-analytical differential transform method. Composites Part B: Engineering, 79, pp.156-169.
24. Ebrahimi, F. and Salari, E., 2015. Thermo-mechanical vibration analysis of nonlocal temperature-dependent FG nanobeams with various boundary conditions. Composites Part B: Engineering, 78, pp.272-290.
25. Nejad, M.Z., Hadi, A. and Rastgoo, A., 2016. Buckling analysis of arbitrary two-directional functionally graded Euler–Bernoulli nano-beams based on nonlocal elasticity theory. International Journal of Engineering Science, 103, pp.1-10.
26. Ansari, R., Oskouie, M.F., Gholami, R. and Sadeghi, F., 2016. Thermo-electro-mechanical vibration of postbuckled piezoelectric Timoshenko nanobeams based on the nonlocal elasticity theory. Composites Part B: Engineering, 89, pp.316-327.
27. Ebrahimi, F. and Salari, E., 2015. Thermo-mechanical vibration analysis of nonlocal temperature-dependent FG nanobeams with various boundary conditions. Composites Part B: Engineering, 78, pp.272-290.
28. Nguyen, N.T., Hui, D., Lee, J. and Nguyen-Xuan, H., 2015. An efficient computational approach for size-dependent analysis of functionally graded nanoplates. Computer Methods in Applied Mechanics and Engineering, 297, pp.191-218.
29. Shafiei, N., Mirjavadi, S.S., MohaselAfshari, B., Rabby, S. and Kazemi, M., 2017. Vibration of two-dimensional imperfect functionally graded (2D-FG) porous nano-/micro-beams. Computer Methods in Applied Mechanics and Engineering, 322, pp.615-632.

30. Chakraborty, A., Gopalakrishnan, S. and Reddy, J.N., 2003. A new beam finite element for the analysis of functionally graded materials. International Journal of Mechanical Sciences, 45(3), pp.519-539.
31. Eltaher, M.A., Emam, S.A. and Mahmoud, F.F., 2012. Free vibration analysis of functionally graded size-dependent nanobeams. Applied Mathematics and Computation, 218(14), pp.7406-7420.
32. Eltaher, M.A., Emam, S.A. and Mahmoud, F.F., 2013. Static and stability analysis of nonlocal functionally graded nanobeams. Composite Structures, 96, pp.82-88.
33. Aria, A.I. and Friswell, M.I., 2018. A nonlocal finite element model for buckling and vibration of functionally graded nanobeams. Composites Part B: Engineering.
34. Bourbié, T., Coussy, O. and Zinszner, B., 1987. Acoustics of porous media: Editions Technip.
35. Sallica-Leva, E., Jardini, A.L. and Fogagnolo, J.B., 2013. Microstructure and mechanical behavior of porous Ti–6Al–4V parts obtained by selective laser melting. Journal of the mechanical behavior of biomedical materials, 26, pp.98-108.
36. Ahmadi, S.M., Campoli, G., Yavari, S.A., Sajadi, B., Wauthlé, R., Schrooten, J., Weinans, H. and Zadpoor, A.A., 2014. Mechanical behavior of regular open-cell porous biomaterials made of diamond lattice unit cells. Journal of the mechanical behavior of biomedical materials, 34, pp.106-115.
37. Biener, J., Hodge, A.M., Hayes, J.R., Volkert, C.A., Zepeda-Ruiz, L.A., Hamza, A.V. and Abraham, F.F., 2006. Size effects on the mechanical behavior of nanoporous Au. Nano letters, 6(10), pp.2379-2382.
38. Bo, J., 1999. The vertical vibration of an elastic circular plate on a fluid-saturated porous half space. International Journal of Engineering Science, 37(3), pp.379-393.
39. Yamaguchi, T., Kurosawa, Y. and Enomoto, H., 2009. Damped vibration analysis using finite element method with approximated modal damping for automotive double walls with a porous material. Journal of Sound and Vibration, 325(1-2), pp.436-450.
40. Leclaire, P., Horoshenkov, K. and Cummings, A., 2001. Transverse vibrations of a thin rectangular porous plate saturated by a fluid. Journal of Sound and Vibration, 247(1), pp.1-18.
41. Vashishth, A.K. and Gupta, V., 2009. Vibrations of porous piezoelectric ceramic plates. Journal of Sound and Vibration, 325(4-5), pp.781-797.
42. Altintas, G., 2014. Natural vibration behaviours of heterogeneous porous materials in micro scale. Journal of Vibration and Control, 20(13), pp.1999-2005.
43. Takahashi, D. and Tanaka, M., 2002. Flexural vibration of perforated plates and porous elastic materials under acoustic loading. the Journal of the Acoustical Society of America, 112(4), pp.1456-1464.
44. Barati, M.R. and Zenkour, A.M., 2018. Electro-thermoelastic vibration of plates made of porous functionally graded piezoelectric materials under various boundary conditions. Journal of Vibration and Control, 24(10), pp.1910-1926.
45. Sahmani, S., Aghdam, M.M. and Rabczuk, T., 2018. Nonlinear bending of functionally graded porous micro/nano-beams reinforced with graphene platelets based upon nonlocal strain gradient theory. Composite Structures, 186, pp.68-78.

46. Sahmani, S., Aghdam, M.M. and Rabczuk, T., 2018. Nonlocal strain gradient plate model for nonlinear large-amplitude vibrations of functionally graded porous micro/nano-plates reinforced with GPLs. Composite Structures, 198, pp.51-62.
47. Khoei, A.R., Vahab, M. and Hirmand, M., 2018. An enriched–FEM technique for numerical simulation of interacting discontinuities in naturally fractured porous media. Computer Methods in Applied Mechanics and Engineering, 331, pp.197-231.
48. Mobasher, M.E., Berger-Vergiat, L. and Waisman, H., 2017. Non-local formulation for transport and damage in porous media. Computer Methods in Applied Mechanics and Engineering, 324, pp.654-688.
49. Na, S. and Sun, W., 2017. Computational thermo-hydro-mechanics for multiphase freezing and thawing porous media in the finite deformation range. Computer Methods in Applied Mechanics and Engineering, 318, pp.667-700.
50. Touloukian, Y.S., 1966. Thermophysical properties of high temperature solid materials. Volume 1. Elements. -Pt. 1. Ed. Yeram Sarkis Touloukian. Macmillan,
51. Shen, H.S., 2016. Functionally graded materials: nonlinear analysis of plates and shells. CRC press.
52. Arash, B. and Ansari, R., 2010. Evaluation of nonlocal parameter in the vibrations of single-walled carbon nanotubes with initial strain. Physica E: Low-dimensional Systems and Nanostructures, 42(8), pp.2058-2064
53. Arash, B., Rabczuk, T. and Jiang, J.W., 2015. Nanoresonators and their applications: a state of the art review.
54. Duan, W.H., Wang, C.M. and Zhang, Y.Y., 2007. Calibration of nonlocal scaling effect parameter for free vibration of carbon nanotubes by molecular dynamics. Journal of applied physics, 101(2), p.024305
55. Kim, Y.W., 2005. Temperature dependent vibration analysis of functionally graded rectangular plates. Journal of Sound and Vibration, 284(3-5), pp.531-549.
56. Kahya, V. and Turan, M., 2017. Finite element model for vibration and buckling of functionally graded beams based on the first-order shear deformation theory. Composites Part B: Engineering, 109, pp.108-115.
57. Wattanasakulpong, N., Prusty, B.G. and Kelly, D.W., 2011. Thermal buckling and elastic vibration of third-order shear deformable functionally graded beams. International Journal of Mechanical Sciences, 53(9), pp.734-743.
58. Ebrahimi, F. and Barati, M.R., 2016. Vibration analysis of nonlocal beams made of functionally graded material in thermal environment. The European Physical Journal Plus, 131(8), p.279.

- A 5-noded beam finite element is proposed to analyse thermo-elastic behaviour of functionally graded porous nanobeams.
- Nonlocal elasticity theory is employed to incorporate the size-dependent behaviour of the nanobeams.
- The finite element procedure and variational formulation are described in detail.
- The axial and shear behaviour of the elastic foundation are considered based on Winkler-Pasternak model.
- The critical buckling temperature and the natural frequencies are calculated for various, porosity distributions, temperature gradients, nonlocal parameters and boundary conditions.